Power Management Unit for Long-Range Harvester-Assisted Wireless Sensor Node

PROYECTO

presentado para optar

al Título de Grado en Ingeniería en Electrónica Industrial por

"Íñigo Fernández de Angulo Barrera"

bajo la supervisión de

"Andoni Beriain Rodríguez"

Donostia-San Sebastián, julio de 2023

Tecnun
Universidad
de Navarra
ESCUELA DE INGENIERÍA
INGENIARITZA ESKOLA
SCHOOL OF ENGINEERING

Tecnun
Universidad
de Navarra
ESCUELA DE INGENIERÍA
INGENIARITZA ESKOLA
SCHOOL OF ENGINEERING

Proyecto Fin de Grado

INGENIERIA EN ELECTRÓNICA INDUSTRIAL

POWER MANAGEMENT UNIT FOR LONG-RANGE HARVESTER-ASSISTED WIRELESS SENSOR NODE

Íñigo Fernández de Angulo Barrera

Donostia-San Sebastián, julio de 2023

Pº Manuel Lardizabal, 13. 20018 Donostia-San Sebastián, Gipuzkoa
Tel. 943 219 877 · Fax 943 311 442 · www.tecnun.es

ACKNOWLEDGEMENTS

First of all, I would like to thank all the people without whom this project could not have been done. Thanks to their support and help, I have overcome the difficulties that have arisen through the development of this project.

Specially, I would like to thank my supervisor Andoni Beriain, who has guided me throughout the whole project, offering great help and being always available to solve my doubts.

I cannot forget to mention my project teammates Xabier Borrajeros, Mario Ibarrola, Aiora Etxeburua and Ignacio Jiménez, who have also done an excellent work and were always there to give me the feedback I needed.

Finally, I would like to thank my family, whose effort has made it possible for me to study this degree, thus giving me an immense chance.

CONTENTS

FIGURES

TABLES

1. ABSTRACT

Energy harvesting has become increasingly important nowadays. This solution allows the development of autonomous devices, avoiding the use of batteries, that do not have a large duration and can be harmful to the environment.

Some energy harvesters provide very low voltages, that are therefore unable to supply what is required by some electronic devices. This can be solved with the use of step-up voltage converters.

Moreover, some of these are not able to provide enough power for continuously supply to sensor nodes. With the help of a voltage monitor we can ensure that the power is only transferred to the sensor node whenever the capacitor storing the energy provided by the harvester is charged enough.

In this work, a Power Management Unit (PMU) for a long-range harvester-assisted wireless sensor node is proposed. The PMU is able to adapt the output voltage of the harvester to the required voltage for the sensor node, and store its energy in a capacitor. It also ensures that power transmission only occurs when the capacitor is charged enough.

2. INTRODUCTION

2.1. Context

The Internet of Things (IoT) is an increasingly important matter in industry. Thanks mainly to the development of internet connectivity and data analysis, many types of objects or devices can now be connected among each other through the internet, thus ameliorating the control we have over them, and the coordination among them.

In terms of impact, it is expected that by 2025 a total of a 100 billion devices will be IoT connected, and their impact on economy will be of more than $ 11 trillion [1]. The solutions provided by this technology have the potential to be used in many different fields, for example in industry, health care, home automation or physical urban infraestructure [2] [3].

An example of IoT systems are sensor networks, where different sensor nodes are continuously generating data or gathering information. This information can be processed or directly shared, because of their internet connectivity. The internet communication allows a computer to process, monitor or control this sensor network. [1]

Sometimes these sensor networks need to be wireless, specially if sensors need to be placed in spaces where wires cannot reach. Autonomous sensor nodes are able to make measurements and send information without the need of being connected with cables. A typical way of implementing autonomous sensor nodes is to power them with batteries. However, this implementation usually prevents the sensor networks from being cheap, durable, reliable and having a high transmission rate at the same time, forcing the designer to sacrifice one of these goals [4]. Battery-powered sensor nodes usually need to implement duty cycle strategies, this is, reducing transmission rates (communication is usually the most energy-consuming task in wireless sensor networks [5]) in order to save energy, helping to increase the durability of the batteries. In addition, they usually become the most expensive part of the system, since they need to be replaced or charged periodically [6].

The emerging technology of energy harvesting is helping with the energy scarcity issue. Energy harvesters convert different types of energies available in the environment (solar, thermal, vibration...), into electrical energy. Energy harvesters can also be combined with duty cycling techniques when the power provided by them is limited. These energy sources can be connected to batteries or capacitors that store energy until the transmission of information is done by the autonomous sensor node. This way, the system can ensure it has enough energy when a consumption peak is required. Using this technology for wireless sensor nodes can

reduce the duty cycle (compared to the one with batteries) if there is enough energy available and the harvester is able to convert it efficiently. [7]

Energy harvesters are not always able to provide the voltage required by the sensor node. A solution to this issue is to implement a DC-DC converter stage before the sensor node, to raise the voltage output of the harvester. This is common for different types of harvesters, like solar cells [8], or thermoelectric generators (TEG) [9].

The power provided by energy harvesters is dependent on dynamic environmental conditions. For example, solar cells do not generate as much energy on sunny days as on cloudy days. The minimum duty cycle for a sensor node depends on the time it takes to charge the battery enough to complete a full transmission of the information that is being collected. For this reason, in order to minimize the time lapse between transmissions, it is desirable to adapt it to the energy that is being provided at each moment by the harvester. This can be done with the use of a battery monitor, which is able to close a switch that connects the capacitor or the battery to the load only when the former has enough energy stored. This way, duty cycle can be adapted to the dynamic environmental conditions. [10]

2.2. Background

This work is part of a bigger project, where the goal is to design a long-range harvester-assisted wireless sensor node. This device should be able to read data from a sensor and send it only using the energy obtained through harvesting techniques. In the project, the maximum communication distance will be calculated, together with the viability on different environments. Figure 1 shows the block diagram of the complete system, this is, including also the block that is in charge of receiving the information that is being generated by the sensor node.

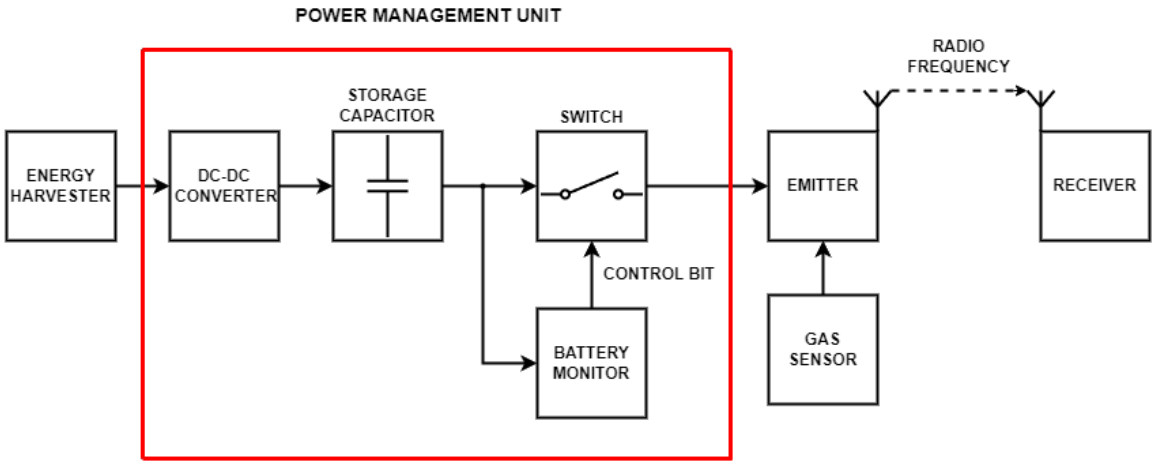

Figure 1: Long-Range Harvester-Assisted Wireless Sensor System Block Diagram

First, an energy harvester will convert energy extracted from the environment into electrical energy. Two options are being evaluated for this device: a solar cell and a Thermoelectric

Generator. The output voltage of the harvester is later adapted by a DC-DC converter to the voltage required by the system. Energy is then stored into a capacitor. A battery monitor controls a switch that allows the energy to be transferred from the capacitor to the emitter only when the capacitor is charged enough. A gas sensor measures the amount of gas in the environment, and this information is read by the emitter (CC1310 sun 1GHz board). The emitter is periodically sending the read information to a receiver, which is connected to the internet and power supply, and can store the received sensor data in the cloud. All the mentioned modules except for the receiver form the autonomous sensor node.

This work is focused on the design of the Power Management Unit of the long-range harvester-assisted wireless sensor node, which includes 4 modules: the voltage converter, the energy storage capacitor, the battery monitor and the switch. Some specifications have been defined for each of these modules:

- The DC-DC step-up converter should be able to provide an output voltage of 3.3 V when no load is connected to it. This is because in this project, the LAUNCHXL-CC1310 Evaluation Board has been chosen for the emitter, and it is the maximum voltage it can operate with. The sensor and its corresponding amplifier receive the power through this board and not directly from the PMU.
- The monitor should close the switch once the voltage across the capacitor reaches the specified value (3.3 V). The monitor should also consume very low power, since a large consumption would make the device counterproductive. When the emitter turns on and starts reading the information of the sensor and transmitting it, the capacitor starts discharging and the voltage across it starts dropping. The monitor should open the switch to prevent the voltage from dropping below 2 V, which is the minimum operation voltage of the CC1310.
- The capacitor should be able to store enough energy for transmissions to occur, but also charge as fast as possible to reduce the time between transmissions, which should be less than a minute.
- The voltage drop across the switch when it is closed should be the minimum possible. The current across the switch when it is open should also be the minimum possible.

3. OBJECTIVES

The main objective in this work is to design a Power Management Unit for a long-range harvester-assisted wireless sensor node. To accomplish this, an iterative incremental design method will be followed. This is, some intermediate designs will be proposed, where the modules that form the PMU (the voltage converter, the battery monitor, the capacitor and the switch) will be added step by step. The objectives of each intermediate design are defined later in this chapter.

An additional objective is to design the Printed Circuit Board (PCB) that implements in a single board all the blocks that appear in Figure 1, except for the receiver, thus integrating the complete long-range harvester-assisted wireless sensor node.

3.1. Design 1: The Voltage Converter and the Capacitor

The main objective is to design two DC-DC Step-Up converters that will adapt the output voltage of the harvesters. The first will be designed for a thermoelectric generator, whereas the second one will be designed for a solar cell. To achieve this, some secondary objectives have been defined.

The first secondary objective is to analyze the different existing ways of boosting DC voltage. This objective includes analyzing what components can be found in the market (or in the laboratory where the project is taking place) that are capable of doing this.

The second objective is to choose which of the analyzed components accomplishes better the defined specifications.

The third objective is to design an adequate PCB for the voltage converter module, using the selected component.

The fourth objective is to test and characterize different parameters of the designed board: its capability of reaching the desired voltage, the maximum current that can be supplied by the designed device in different environmental conditions that affect the amount of energy that the harvesters can provide, and the amount of time it takes to reach the desired voltage. The latter depends on the value of the storage capacitor and the load, so different capacitor and load values will be tested.

The fifth objective is to determine which is more adequate: the solar cell or the thermoelectric generator.

The last objective is to define the redesign criteria that is to be used for the second design.

3.2. Design 2: The Battery Monitor

The main objective in the second design is to add the battery monitor module to the first design. To achieve this, some secondary objectives have been defined.

The first secondary objective is to analyze different options available in the market (or in the laboratory where the project is taking place) that are able to monitor the voltage across a capacitor.

The second objective is to choose the component that accomplishes better the defined specifications.

The third objective is to design an adequate PCB for the voltage converter module and the battery monitor module, using the selected component for voltage monitoring and applying the redesign criteria defined for the previous design (Design 1).

The fourth objective is to test and characterize different parameters of the design, like the maximum transmit burst rate on different environmental conditions.

The last objective is to define the redesign criteria that is to be used for the third design.

3.3. Design 3: The Switch

The main objective in the third design is to complete the PMU adding the last remaining module: the switch. To achieve this, some secondary objectives have been defined.

The first secondary objective is to analyze different types of switches available in the market or in the laboratory where the project is taking place.

The second objective is to choose the most adequate. For this purpose, more than one switch could be tested. To choose among more than one switch, the voltage drop across them during OFF and ON state will be characterized and compared.

The third objective is to add the selected switch to the second design, or a correction of it applying the defined redesign criteria, thus completing the third design.

The last objective is to define the redesign criteria that is to be used to design the final autonomous sensor node.

4. MAIN COMPONENT SELECTION

In this chapter different ways of implementing each of the modules that form the PMU are analyzed, including some options available in the market, and the final choice for our design is explained.

4.1. DC-DC Step-up Converters and Charge Pumps

It is common for some energy harvesters like TEGs or solar cells to provide low voltages, thus making the use of DC/DC step-up converters crucial for their applications [11] [12]. These devices are able to convert low voltages into high ones by means of different techniques.

There is no unique optimal technique to raise DC voltages, and the selection of it depends on the specific application purpose [13]. For this reason, the different desired properties and characteristics must be analyzed.

Some DC-DC boost converters offer isolation between input and output, like DC-DC flyback converters, however, this is not usually needed for low power applications, and it is also more costly, space-occupying and inefficient. [13] [14]

Another option is having a bidirectional converter. Bidirectional converters are more complex and costly than unidirectional converters, so they should be only used if necessary [13]. This is not the case of energy harvesting and sensor node applications, since power is only transferred in one direction: from the harvester to the sensor node.

It is also important to consider whether the device is voltage-fed or current-fed. For low voltage renewable applications current-fed DC-DC step-up converters are more common [13].

Other limitations might be having low multiplying factors. This can be solved by techniques such as cascading.

Having analyzed the desired properties, it is interesting to analyze the specific techniques that can accomplish this and compare them.

- DC-DC step-up converters use an inductor to store energy that is later transferred to a capacitor to raise the output voltage. Their main advantages are their high efficiency,

low output ripple and being able to reach high voltage multiplication factors. Their main disadvantages are their cost (higher than charge pumps) and the space they occupy (mainly due to the combination of inductor and capacitor) [15]. The latter is not a problem for this project, since there is no space limitation. They also require switches, which can be built using different components such us diodes or transistors. Eric J. Carlson, Kai Strunz, and Brian P. Otis suggest the use of pFETS, to avoid voltage drop and allow inputs as low as 20 mV [16].

- Classical DC-DC charge pumps use switch-capacitor configurations in order to raise the voltage. Their main advantages are that they are very cheap, efficient, and occupy little, since they can be integrated into the power integrated circuit chip [15]. However, they have a limited multiplying factor, and require a threshold voltage that might be too high for some harvesters, like thermoelectric generators. If the problem of the threshold voltage is solved, an advantage of working with integrated circuits is that low leakage currents can be ensured, thus enabling these devices to work with ultralow voltage inputs [17].
- Other options include hybrid inductive and capacitive architectures [18]

We are interested in charging rapidly the capacitor that stores the energy that is later provided to the device. The speed at which it is charged depends on various factors, but an important one is efficiency, since being able not to lose energy along the process will make the capacitor reach a higher energy point faster.

Considering all these aspects, Table 1 shows a list of different options available in the market that could be adequate for the purpose of this work, comparing their main characteristics.

Name:	LTC3108	LTC3105	MAX17227A	BQ25504
Type	Charge pump	Step-up	Step-up	Step-up
Vin min	20 mV	225 mV	400 mV	130 mV
Vin start	20-50 mV	250 mV	880 mV	600 mV
Vin max	500 mV	5V	5.5V	5.5V
Vout	2.35V / 3.3V / 4.1V / 5V	1.6V to 5.25V	2.3 to 5.2 V	2.2V to 5.25V
MPPT [1]	No	No	No	Yes

Table 1: Comparison Between Different DC-DC Step-Up Converters in the Market

4.2. Battery Monitors

Ideally, the input power and the output power of a DC-DC boost converter should be equal. This way, taking into account Equation 1, a higher output voltage would mean a proportionally lower average output current. In some cases, the devices demand more current than the one that can be provided by the DC-DC converter and the harvester. This can be solved using Duty Cycle techniques. These consist in turning the device on and off periodically, so

[1] Maximum Power Point Tracking

that the average current is low enough, even if the demanded current during ON state is too high. Energy can be stored during OFF or Sleep Mode states in a capacitor, and later be released during ON state.

$$P = V * I \tag{1}$$

The power provided by the harvester is not constant and depends on dynamic environmental conditions. The monitor can control a switch to ensure that transmissions only start when the capacitor has enough energy stored, thus minimizing the duty cycle.

Some available examples in the market are the MAX6427, the MAX6433, and the MAX6434. The MAX6427 has factory trimmed thresholds. This means that it is not possible to adjust the threshold voltages where the output pin turns on or off. The MAX6433 and the MAX6434, however, have adjustable threshold voltages. Figure 2 shows how the output bit of the monitor (LBO) changes depending on the value of the battery (or capacitor) voltage V_{BATT} compared to the high and low threshold voltages V_{HTH} and V_{LTH}.

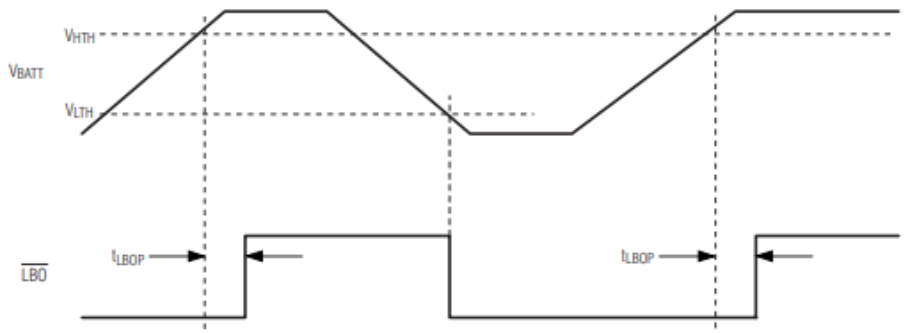

Figure 2: MAX6433 Output Bit $\overline{LBO}$ [19]

The main difference between the MAX6433 and the MAX6434 is that the MAX6433 has an active-low push-pull output while the MAX6434 has an active-low open-drain output [19].[2]

4.3. Switches

Switches are a type of electronic component that is able to open or close a circuit. They can be classified in different ways.

The main technologies with which electronic switches can be built are diodes, transistors and thyristors [20]. Each of them has different properties.

[2]Section 4.2 has been done in collaboration with Ignacio Jiménez

In this project, the objective is to find a fully-controllable switch. Therefore, diodes can be discarded.

The thyristor family of switches is often used for alternate current and relatively high power requirements [20].

Having briefly analyzed the different options, the transistor family of switches has been selected for this project. The reasons for this are that they are fully controllable and can properly work in low power DC applications.

The SN74LVC1G66-Q1 is a single bilateral analog switch that can be controlled through one of its pins, so that when the input voltage in this pin is high, the switch closes, and when it is low, it is open. The ON resistance, r_{on}, is quite low in this device, as it is possible to observe in its Data Sheet [21]. This means that the voltage drop when the switch is closed should be very low. This property is very interesting for this application, since the objective is to supply the closest value to 3.3 V to the emitter and the gas sensor.

In addition, some NPN type Bipolar Junction Transistors (BJT) are available in the laboratory where this project is being done.

4.4. Final Selection

Having analyzed the different options that can be used in the modules of the PMU, the final selection is specified in this section.

Following the example of Hector Solar et al [22], for the voltage converter module, the LTC3108 has been chosen among the options shown in Table 1, mainly because of its capacity to boost voltages as low as 20 mV. TEGs can provide very low voltages if the temperature gradient between the hot side and the cold side of the harvester is very low, thus making the chosen device better suit for these cases.

For the battery monitor, the MAX6433 has been chosen. The main reason is that the threshold voltages are adjustable (which is not the case of the MAX6427), and that it was available in the laboratory at the moment of the board development (which was not the case of the MAX6434).

For the switch, the SN74LVC1G66-Q1 has been chosen, but since some NPN Bipolar Junction Transistors are available in the laboratory, both switches have been selected for testing, to be later compared.

5. DESIGN 1: THE DC-DC CONVERTER AND THE CAPACITOR

In this chapter, a first intermediate design is presented. This design includes the DC-DC converter module, that adapts the output voltage of the harvester to the required one by the emitter board (3.3 V). Moreover, the results of testing and characterizing this design are shown in this chapter. The voltage converter module already includes a storage output capacitor, but the results of using other capacitors in parallel to the one already included have also been analyzed.

Figure 3 shows the block diagram of the complete system. Thick black borders indicate that the block is included in this first intermediate design, while grey thin borders indicate that the block is not included in the design presented in this chapter.

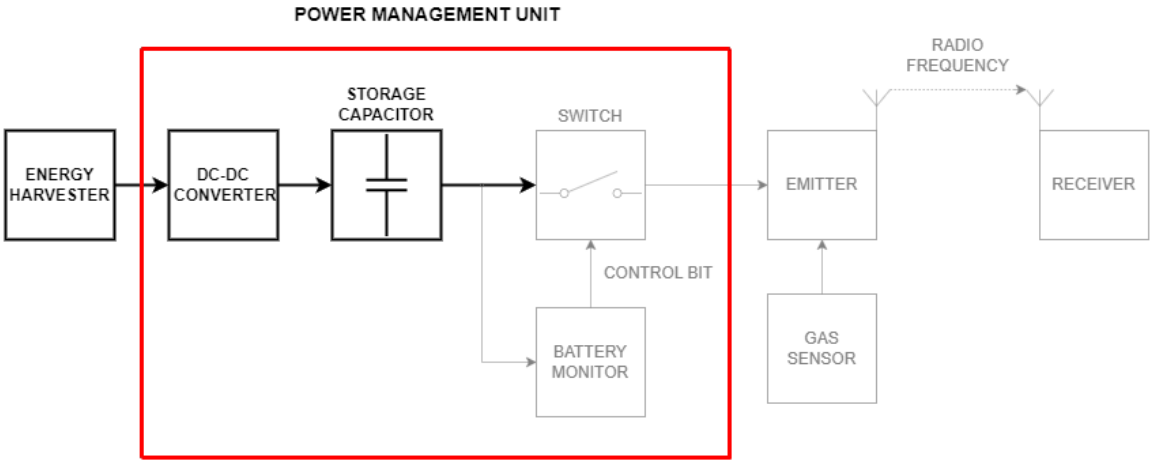

Figure 3: Design 1 Block Diagram

5.1. Design 1 Proposal

In this section, the design of the first PCB and the selection of its components is explained.

The design process has been carried out following the recommendations of the LTC3108 Data Sheet [23].

5.1.1. Design 1 PCB

The LTC3108 can be adapted to different voltage sources by making small changes on the external circuitry required for it to work properly. For this reason, a PCB valid for two types of energy harvesters (a TEG and a solar cell) has been designed. The designed board is the same for both harvesters. However, the value of the components that are soldered to them are different.

Figure 4 shows the schematic of the step-up converter PCB, which is inspired by the examples given in the LTC3108 Data Sheet [23]. Figure 5 shows the actual design of the board.

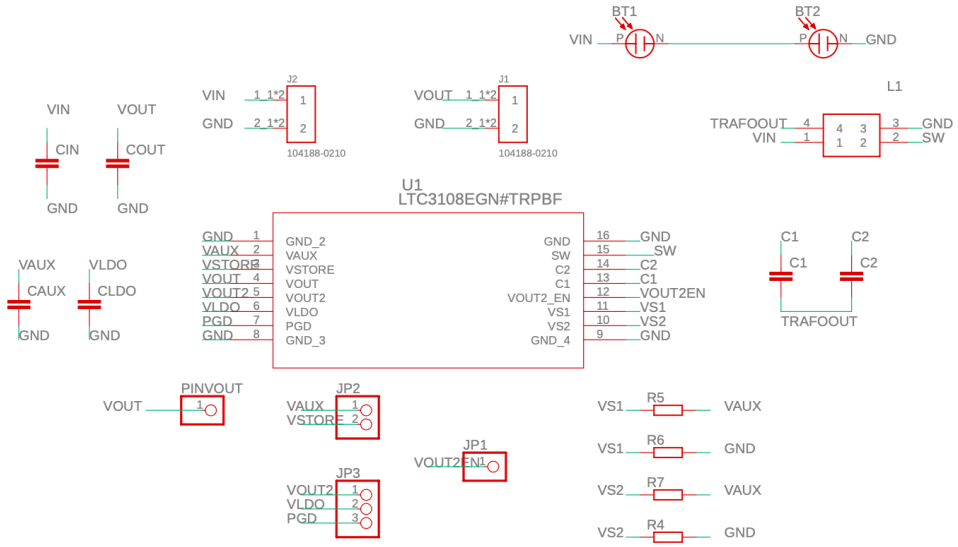

Figure 4: Design 1 Schematic

Initially, the design had the top layer referenced to VAUX, and the bottom layer to GND. However, this layout required more through-holes than doing it the other way round. This is, referencing the top layer to GND, and the bottom layer to VAUX resulted in a cleaner design.

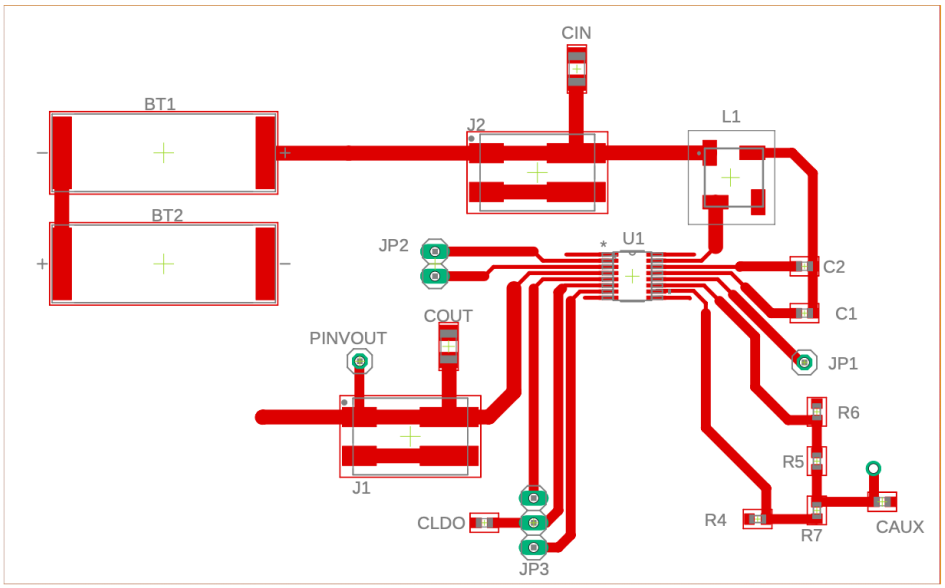

Figure 5: Design 1 Printed Circuit Board

5.1.2. Design 1 Component Selection

Name	Device	TEG value	Solar Cell value
C1	C0603	1 [nF]	10 [nF]
C2	C0603	330 [pF]	330 [pF]
CIN	C1206	220 [µF]	220 [µF]
CLDO	C0603	2.2 [µF]	2.2 [µF]
CAUX	C0603	3.3 [µF]	2.2 [µF]
L1	74488540070 / 74488540250	1:100 [Turn Ratio]	1:20 [Turn Ratio]
JP1	PINHD-1X1	1 [Pins]	1 [Pins]
JP2	PINHD-1X2	2 [Pins]	2 [Pins]
JP3	PINHD-1X3	3 [Pins]	3 [Pins]
J1	104188-0210	2 [Contacts]	2 [Contacts]
J2	104188-0210	2 [Contacts]	2 [Contacts]
R4	R0603	0 [Ω]	0 [Ω]
R5	R0603	0 [Ω]	0 [Ω]
R6	R0603	0 [Ω]	0 [Ω]
R7	R0603	0 [Ω]	0 [Ω]
COUT	C1206	100 [µF]	100 [µF]
BT1	KXOB25-05X3F	Not used	Not relevant
BT2	KXOB25-05X3F	Not used	Not relevant

Table 2: Design 1 Bill of Materials

Table 2 shows the list of components needed to complete the circuit. On the left column the name indicating the position of the component on both the schematic and the board [Figures 4 and 5] is written. The second column, shows the name of the device that corresponds into that position. The third column, shows the value of each component regarding the TEG board, while the right column shows the value corresponding to the solar cell board.

BT1 and BT2 are the spaces where the KXOB25-05X3F, the selected solar cell model for this project, can be soldered. They are not used in the board designed for the TEG.

The chosen values for C1, C2, CIN, CLDO and CAUX are the recommended ones in the LTC3108 Data Sheet [23]. CIN is not strictly necessary, but it is recommended, since it does help to stabilize the input voltage, thus improving performance.

When the TEG's temperature gradients between the hot and the cold side are low, the output voltage can also be very low [22]. Using the 1:100 turn ratio transformer allows to work with voltages as low as 20 mV [23]. Solar cells are more likely to have a higher output voltage, thus allowing the use of lower turn ratio transformers. L1 corresponds to the pad where the transformers are placed. The transformer models chosen for the project are the Wurth Elektronik 74488540250 (1:20 turn ratio) for the TEG board and the Wurth Elektronik 74488540070 (1:100 turn ratio) for the solar cell board. These models are also the recommended ones in the LTC3108 Data Sheet. Both of them share the same footprint, so any of them can be soldered correctly in the designed board.

JP1, JP2 and JP3 are male pin headers. JP1, JP2 and JP3 are not strictly necessary for this project, but have been included for other future uses of the board.

J1 and J2 are female board connectors that allow a more stable connection than pins. They are used for the input and output voltages.

In addition, some pads for 0 Ω resistors (R4, R5, R6 and R7) have been added in the PCB. With these, VS1 and VS2 can be independently connected to either ground or VAUX. This determines the output voltage of the device. In this project, VS1 is connected to VAUX, while VS2 is connected to ground, to ensure an output voltage of 3.3V, our objective. However, the pads to connect VS1 to ground or VS2 to VAUX have been added, so that the board has flexibility to test different configurations in the future.

COUT is the energy storage capacitor. The LTC3108 does not immediately provide the chosen voltage output without it. A test was carried out without COUT and the system was unable to provide any voltage. The optimal value of this capacitor can be obtained with Equation 2 [23]:

$$C_{OUT} = \frac{I_{average} * T_{transmission}}{V_{maxdrop}} \tag{2}$$

Where $I_{average}$ is the average current required by the sensor node during transmissions; $T_{transmission}$, the time lapse between transmissions (transmit burst rate); and $V_{maxdrop}$ the maximum voltage drop allowed. Since the current that is consumed by the sensor node is unknown, a capacitor of 100 µF has been chosen.

5.2. Design 1 Testing and Characterization

With the proposed design, different variables can be measured to determine whether the design is apt for our purpose. In this sections, the different set-ups that have been used to make the different measurements are explained, together with the obtained results.

5.2.1. The Output Voltage: VOUT

VOUT using the TEG Set Up

To test the board together with the TEG, a temperature gradient must be created between both sides of the generator. This is possible using the set up shown in Figure 6. The 6.11 Ω resistor is connected to a DC voltage source. This way, current passing through the resistor causes its temperature to rise, until it reaches thermal equilibrium, which occurs when the heat generated by it ($P = I^2 * R$) equals the one dissipated from the resistor's surface. The resistor has a flat surface on top of which the TEG can rest. This way, the"hot" side of the TEG is in direct contact with the resistor, while the"cold" side is in contact with the air in the room, which is cooled with an Air Conditioning (AC) System.

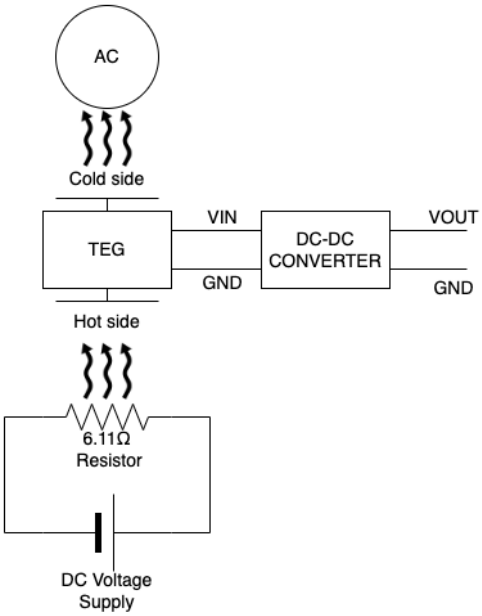

Figure 6: VOUT Testing Set-Up With the Thermoelectric Generator

VOUT Using the Solar Cell Set Up

To test the Solar Cell, two KXOB25-05X3F Solar Cells have been soldered in the board. To test them it is important to take into account the amount of light they can receive in different environments. For this reason, they have been tested both indoors with the artificial light

inside the laboratory, and outdoors, leaving them outside a window so that sunlight could reach them.

VOUT Measurement Results

With the help of a multimeter, it has been proven that the designed board for the TEG works as expected. The output voltage, VOUT, is not the desired one immediately after connecting the DC-DC converter to the TEG, and it was observed that the time it took to reach the desired voltage depended on the temperature gradient.

In the case of the board designed for the solar cell, it has been observed that it does not work as expected. The system was unable to provide the desired output voltage. In Chapter 9, some hypothesis that could explain this are discussed, that could be studied in future work.

5.2.2. Thermal Noise

During testing, it was observed that the room temperature, cooled with an AC system, oscillated somewhat through time. This affected directly the gradient between both sides of the TEG, making it necessary to measure how big its influence was.

Thermal Noise Characterization Set Up

To do so, a DC voltage supply of 5 V was applied on the resistor shown in Figure 7. After leaving it for an hour to avoid the transient before thermal equilibrium, measures of the temperature on both the “hot” and the “cold” side of the TEG were taken, using a multimeter and a Type K thermocouple. The measures were repeated some hours later, to confirm that it had actually reached thermal equilibrium.

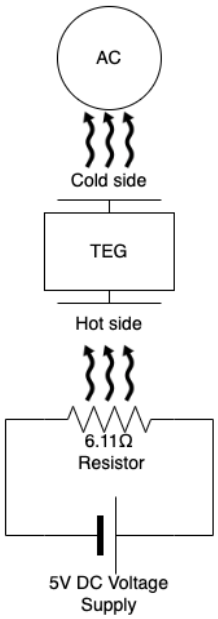

Figure 7: Thermal Noise Characterization Set-Up

Thermal Noise Characterization Results

Figure 8 shows the results of measuring the temperature gradients in the two different moments of the day. The graph shows that the oscillations are high. The fact that the average is almost the same at both times of the measurements confirms that both measurements were taken when the Set-Up had already reached thermal equilibrium.

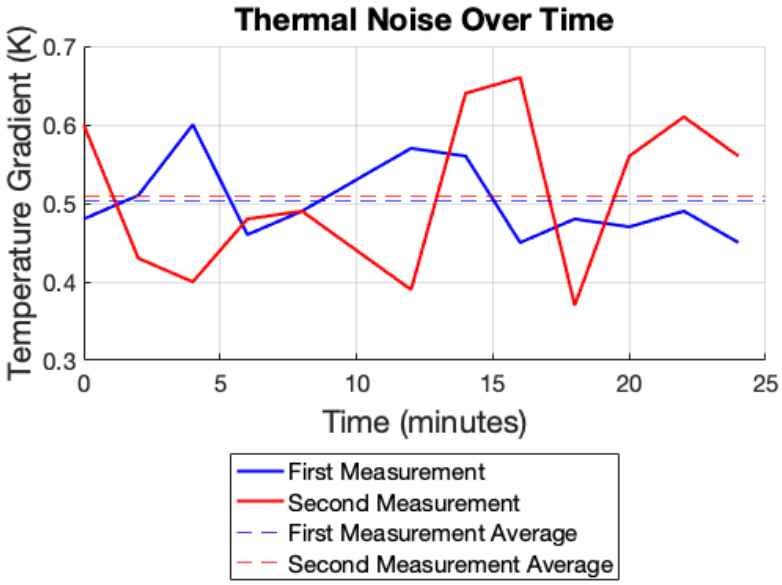

Figure 8: Thermal Noise over Time

5.2.3. Maximum Output Current

Maximum Output Current Characterization Set Up

It is important to understand how much current can the TEG combined with the DC-DC step-up converter provide to the load on different conditions. The power that can be supplied by the TEG is limited by the temperature gradient between the hot and the cold side. Maximum current can be measured with the use of a variable resistor. Testing how low this variable resistor could be before the output voltage was a 10% lower (this is, lower than 2.7V) it has been possible to calculate the maximum current with Ohm's Law ($I_{max} = V/R_{min}$). The set up for this measurement is shown in Figure 9:

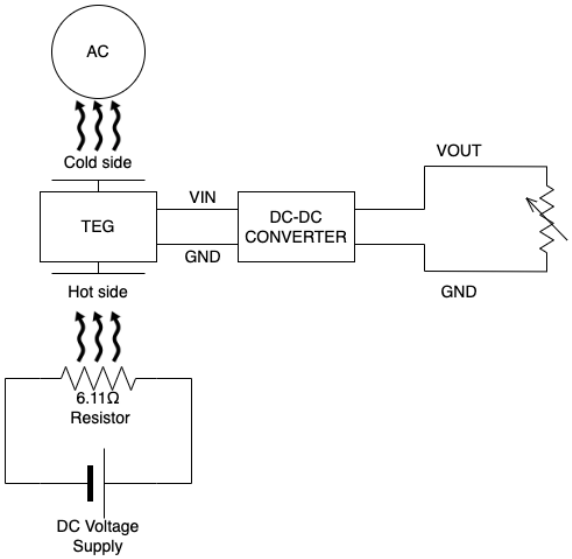

Figure 9: Maximum Current Measurement Set-Up

Maximum Output Current Characterization Results

Figure 10 shows the maximum current that can be provided by the TEG and the DC-DC step-up converter together, allowing a 10% voltage drop, this is, an output voltage of the DC-DC step-up converter of 2.7 V.

It is possible to appreciate in Figure 10 that very low temperature gradient variations have a considerable impact on the maximum output current.

Analyzing Figure 8 together with Figure 10 it is possible to appreciate the limitations of the latter. The thermal noise in the laboratory where these results were obtained could have been enough to noticeably alter them. Finding a more adequate environment where the temperature gradient noise could be reduced was not possible during the execution of this project.

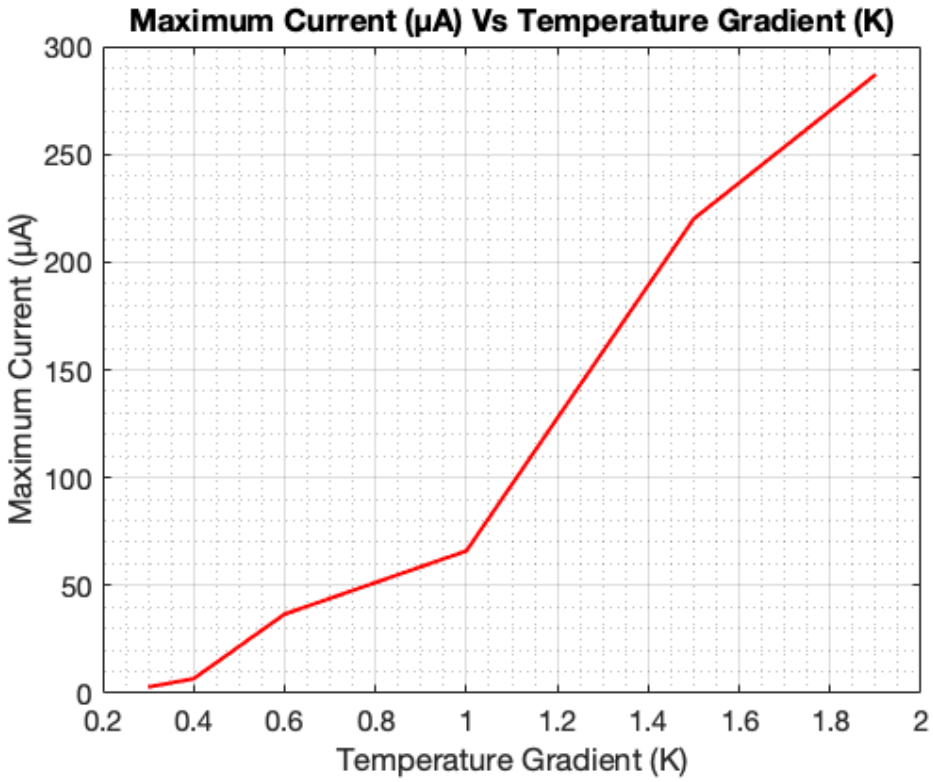

Figure 10: Maximum Output Current (µA) vs Temperature Gradient (K) (2.7 V output)

5.2.4. Output Voltage (VOUT) Charging Time

The t_{VOUT}, this is, the time it takes the output voltage of the converter (VOUT) to reach the programmed voltage for the first time (starting from 0 V), could be calculated using Equation 3, as proposed in the LTC3108 Data Sheet [23]:

$$t_{VOUT} = \frac{V_{outProgrammed} * C_{OUT}}{I_{CHG} - I_{VOUT} - I_{LDO}} + t_{LDO} \tag{3}$$

Where $V_{outProgrammed}$ is the programmed output voltage, I_{CHG}, the charge current; I_{VOUT}, the load current on VOUT; I_{LDO}, the load current on LDO; and t_{LDO}, the time it takes LDO to reach regulation. The latter can be calculated with Equation 4:

$$t_{LDO} = \frac{V_{LDO} * C_{LDO}}{I_{CHG} - I_{LDO}} \tag{4}$$

Where V_{LDO} equals 2.2 V; and C_{LDO}, 2.2 µF.

However, the current I_{CHG} is unknown. The t_{VOUT} can still be measured empirically using an oscilloscope.

VOUT Charging Time Measurement Set Up

Figure 11 shows the set up to do these measurements. The DC Voltage source is providing 5 V. The system is providing current to both a capacitor and a resistor. The experiment has been carried out combining different values for both the capacitor and the resistor.

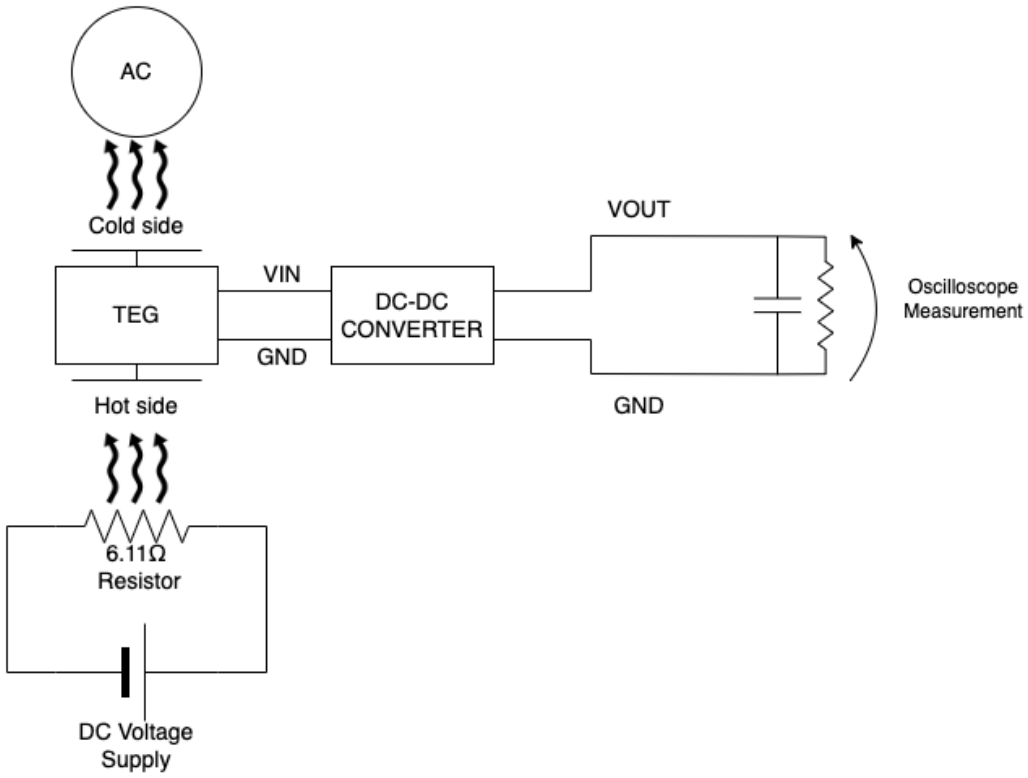

Figure 11: VOUT Charging Time for the First Time Set-Up

VOUT Charging Time Measurement Results

With an oscilloscope, the time it took to charge different capacitors for the first time in parallel with different resistor loads was measured, thus obtaining Table 3:

The highlighted time values in the table show results that seem incoherent with the rest of the results. Ideally, a 5 MΩ load should help the capacitor charge faster, since it reduces the current that goes to the load. However, this is not the case. In this work, the proposed hypothesis to explain this is that thermal noise, which was analyzed in Figure 8, is noticeably affecting the power generated by the TEG, thus having made the capacitor charge faster even if the load was of a lower value.

In Figure 12 it is observed that the slope is steeper for the 2 MΩ load than for the 5MΩ load, even if theoretically it should be the opposite. The graphs showing VOUT vs Time with the different resistors and capacitors that appear on the table have been included in

0 to 1.8 V	10 µF	47 µF	100 µF
0.47 MΩ	5.25 s	6.65 s	9.82 s
1 MΩ	4.90 s	6.73 s	9.27 s
2 MΩ	4.84 s	6.73 s	7.35 s
5 MΩ	5.28 s	5.97 s	7.87 s

(a) Time for VOUT to go from 0 V to 1.8 V

1.8 to 3.3 V	10 µF	47 µF	100 µF
0.47 MΩ	5.38 s	6.69 s	10.07 s
1 MΩ	4.80 s	6.57 s	9.09 s
2 MΩ	4.52 s	6.26 s	6.99 s
5 MΩ	4.66 s	5.52 s	7.27 s

(b) Time for VOUT to go from 1.8 V to 3.3 V

0 to 3.3 V	10 µF	47 µF	100 µF
0.47 MΩ	10.63 s	13.34 s	19.89 s
1 MΩ	9.70 s	13.30 s	18.36 s
2 MΩ	9.36 s	12.99 s	14.34 s
5 MΩ	9.94 s	11.49 s	15.14 s

(c) Time for VOUT to go from 0 V to 3.3 V

Table 3: Vout Charging Time Combining Different Resistors and Capacitors

Appendix A [Figures 34 to 45].These graphs indicate precisely the time where the voltage reaches 1.8 V and 3.3 V for each case.

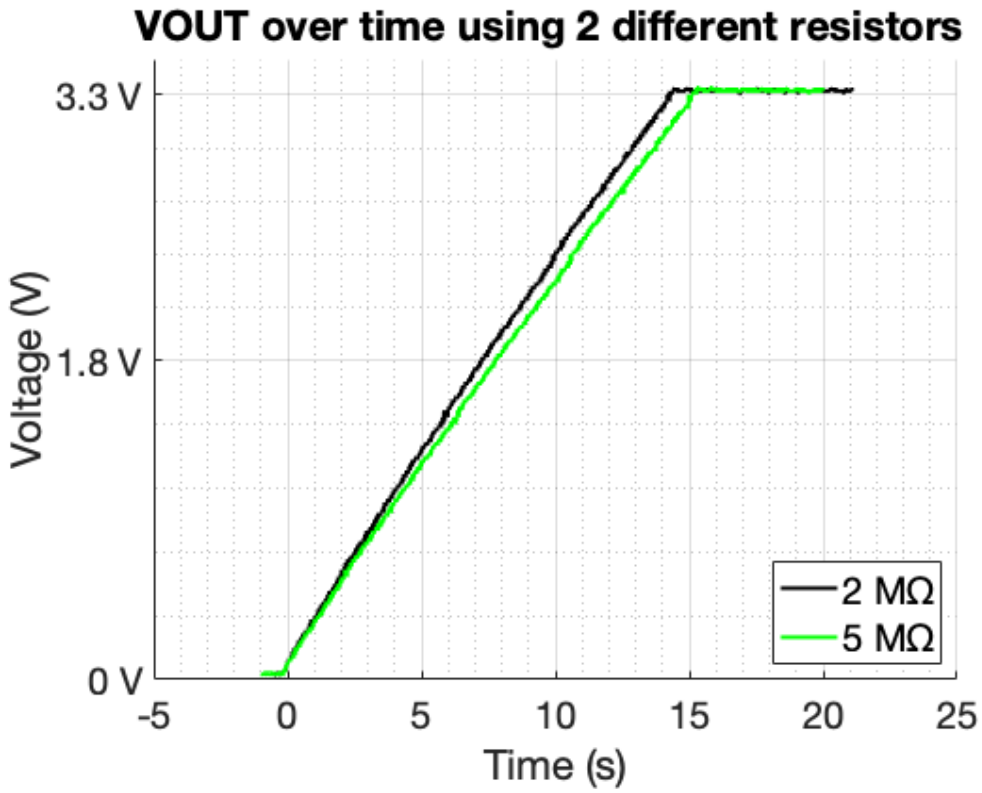

Figure 12: VOUT over Time Using 100 µF Capacitor and 2 Different Resistors

5.3. Summary and Redesign Criteria

In this chapter, two voltage converter module designs have been proposed, one for a TEG and another one for a Solar Cell. The latter, has been tested without obtaining the desired results, while the former has been successfully validated. The maximum output current has been characterized for different temperature gradients. Since some variation on results have been detected, the thermal noise in the room where the testing has taken place has also been characterized. Finally, the time it takes the module to reach the desired voltage has been measured, with different output capacitors to store the energy, and different resistors in parallel to the capacitor acting as loads.

The next chapter describes the second intermediate design. Following an incremental designing method, it includes the voltage converter module described in this chapter together with the energy storage capacitor, and adds a voltage monitor module to it. With the new module, additional testing and characterizing is also described in the following chapter. No changes need to be made in the voltage converter module, which has been successfully implemented.

6. DESIGN 2: THE VOLTAGE MONITOR

In this chapter, a second intermediate design is presented. The design includes the modules that appeared in the previous design, this is the voltage converter and its output energy storage capacitor, and an additional voltage monitor module. The voltage monitor module has an output bit that is HIGH when there is enough energy in the storage capacitor, and LOW when the capacitor requires to be charged, which is when the voltage across it gets lower than 2 V. The results of testing and characterizing this intermediate design are also shown in this chapter.

Figure 13 shows the block diagram of the complete system. Thick black borders indicate that the block is included in this second intermediate design, while grey thin borders indicate that the block is not included in the design presented in this chapter.

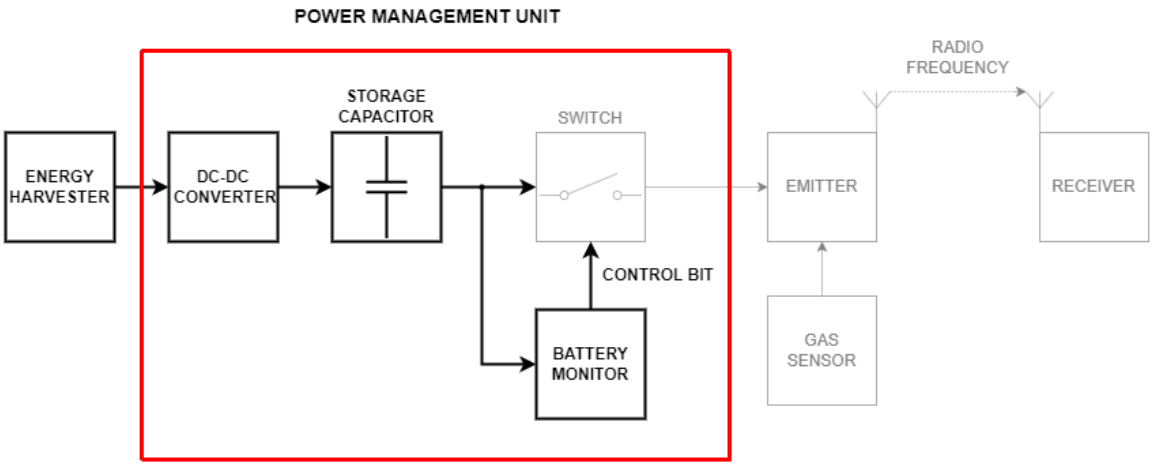

Figure 13: Design 2 Block Diagram

6.1. Design 2 Proposal

The MAX6433 allows to monitor the voltage across a capacitor. The external circuitry required for its correct use has been designed following the recommendations on its Data Sheet [19].

We can see the schematic of the circuitry required for the MAX6433 in Figure 14:

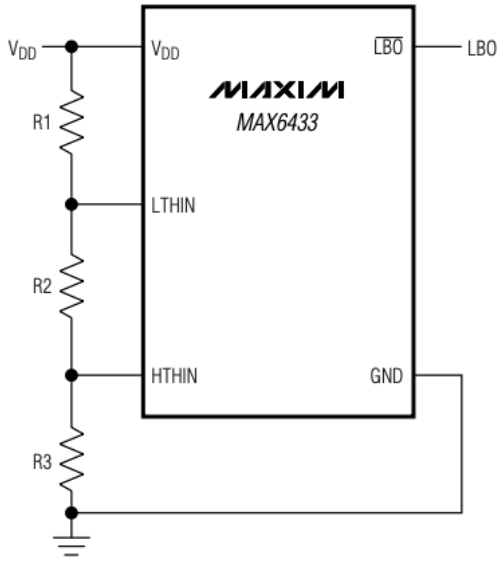

Figure 14: MAX6433 Schematic [19]

6.1.1. Design 2 PCB

The MAX6433 can provide an output bit that is HIGH when it crosses a high voltage thresholds and LOW when it crosses the low voltage threshold. These thresholds are adjustable with the help of external circuitry.

Figure 15 shows the schematics of the PCB of the second design, which combines the schematic of the PCB of the first design [Figure 4] with the schematic required for the MAX6433 battery monitor [Figure 14] . Figure 16 shows the actual design of the second board.

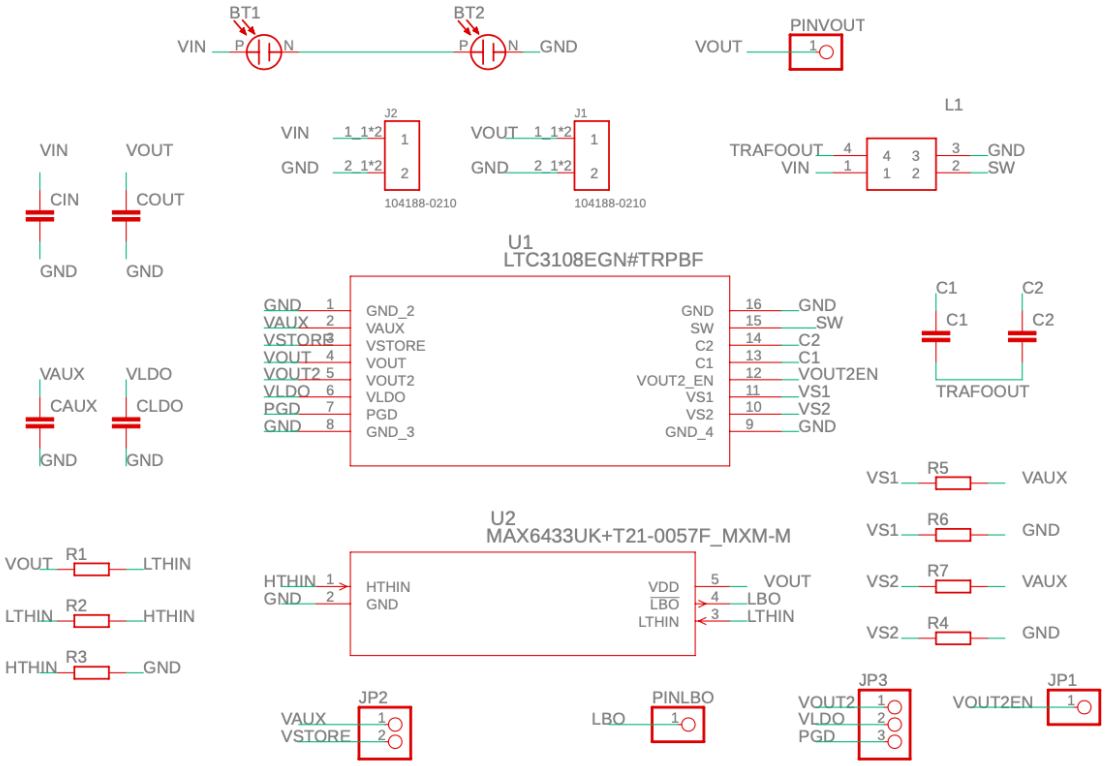

Figure 15: Design 2 Schematic

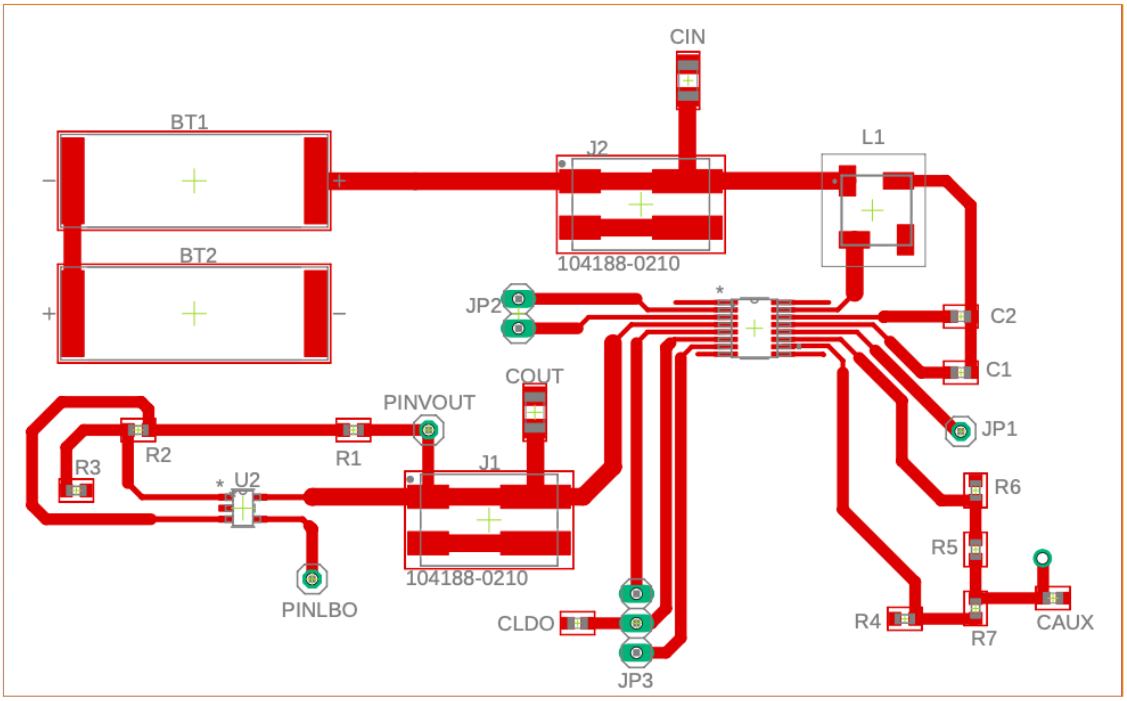

Figure 16: Design 2 Printed Circuit Board

6.1.2. Design 2 Component Selection

Table 2 showed the list of components required for the first design. Table 4 shows the list of components required for the PCB of the second, this is, adding the components that have been introduced in this chapter to the ones that were already present on the previous intermediate design. Again, on the left column the name indicating the position of the component on both the schematic and the board [Figures 15 and 16] is written. The second column, shows the name of the device that corresponds into that position. The third column, shows the value of each component regarding the TEG board, while the right column shows the value corresponding to the solar cell board.

Name	**Device**	**TEG value**	**Solar Cell value**
C1	C0603	1 [nF]	10 [nF]
C2	C0603	330 [pF]	330 [pF]
CIN	C1206	220 [µF]	220 [µF]
CLDO	C0603	2.2 [µF]	2.2 [µF]
CAUX	C0603	3.3 [µF]	2.2 [µF]
L1	74488540070 / 74488540250	1:100 [Turn Ratio]	1:20 [Turn Ratio]
JP1	PINHD-1X1	1 [Pins]	1 [Pins]
JP2	PINHD-1X2	2 [Pins]	2 [Pins]
JP3	PINHD-1X3	3 [Pins]	3 [Pins]
J1	104188-0210	2 [Contacts]	2 [Contacts]
J2	104188-0210	2 [Contacts]	2 [Contacts]
R4	R0603	0 [Ω]	0 [Ω]
R5	R0603	0 [Ω]	0 [Ω]
R6	R0603	0 [Ω]	0 [Ω]
R7	R0603	0 [Ω]	0 [Ω]
COUT	C1206	100 [µF]	100 [µF]
BT1	KXOB25-05X3F	Not used	Not relevant
BT2	KXOB25-05X3F	Not used	Not relevant
U2	MAX6433	Not relevant	Not relevant
R1	R0603	3.6 [MΩ]	3.6 [MΩ]
R2	R0603	560 [kΩ]	560 [kΩ]
R3	R0603	1 [MΩ]	1 [MΩ]
PINLBO	PINHD-1X1	1 [Pins]	1 [Pins]

Table 4: Design 2 Bill of Materials

The selection of the components from row 1 (C1) to row 18 (BT2) has been explained in Subsection 5.1.2.

U2 represents the MAX6433 device, which is the monitor that has been chosen for the project.

R1, R2 and R3 are three resistors required for the monitor, whose values have been calculated following the recommended steps on the MAX6433 Data Sheet [19]:

$$R3 = \frac{V_{REF-} * R_{TOTAL}}{V_{TRIPHIGH}} \tag{5}$$

For Equation 5, we can choose a value for R_{TOTAL} as long as it is equal or lower than 5MΩ. The chosen value for this project is 5MΩ, in order to reduce losses. V_{REF-} is equal to 0.585 V and we want $V_{TRIPHIGH}$ to be 3 V (the reason for not choosing 3.3V is to leave some margin to ensure LBO output can be turned high). This leaves $R3 = 975k\Omega$.

$$R2 = \frac{V_{REF+} * R_{TOTAL}}{V_{TRIPLOW}} - R3 \tag{6}$$

In Equation 6, V_{REF+} is equal to 0.615 V, and we want $V_{TRIPLOW}$ to be 2 V. This leaves $R2 = 562.5k\Omega$.

$$R1 = R_{TOTAL} - R3 - R2 \tag{7}$$

Equation 7 leaves $R1 = 3.4625M\Omega$.

However, the resistors available in the laboratory where the project is taking place have been used, to avoid buying new ones. The most similar values to the calculated ones were:

- $R1 = 3.6M\Omega$
- $R2 = 560k\Omega$
- $R3 = 1M\Omega$

Returning to Equations 5 and 6 we get that our actual maximum and minimum voltages should be of 3.02 V and 2.03 V, respectively.

PINLBO is a male header pin for the output bit of the monitor. Its voltage is HIGH when COUT is charged enough, and LOW while it is charging up.

6.2. Design 2 Testing and Characterization

With the second PCB designed, we can now test the performance of the combination of the voltage converter block together with the voltage monitor block.

6.2.1. Maximum Transmit Burst Rate

Following the LTC3108 Data Sheet [23], the maximum transmit burst rate could be calculated with Equation 8:

$$T = \frac{C_{OUT} * V_{maxdrop}}{I_{CHG} - I_{OUTSLEEP}} \tag{8}$$

Where $I_{OUTSLEEP}$ is the total current drawn from VOUT in the sleep state. Neither this current nor I_{CHG} are known. However, with the help of the monitor, it is possible to know when the capacitor is charged enough to start a transmission.

Maximum Transmit Burst Rate Set Up

Figure 17 shows the set-up required for measuring the maximum burst rate. Connecting the LBO pin (which is high once the capacitor is charged enough, and turns low when the capacitor discharges too much) to a transistor, it is possible to periodically charge and discharge the 100 µF capacitor in parallel to the one included in the design, and whose value is also 100 µF. Using an oscilloscope it is possible to measure how big the time lapse between tranmission is (equivalent to the time it takes the voltage across the capacitor to go from the low threshold voltage to the high one).

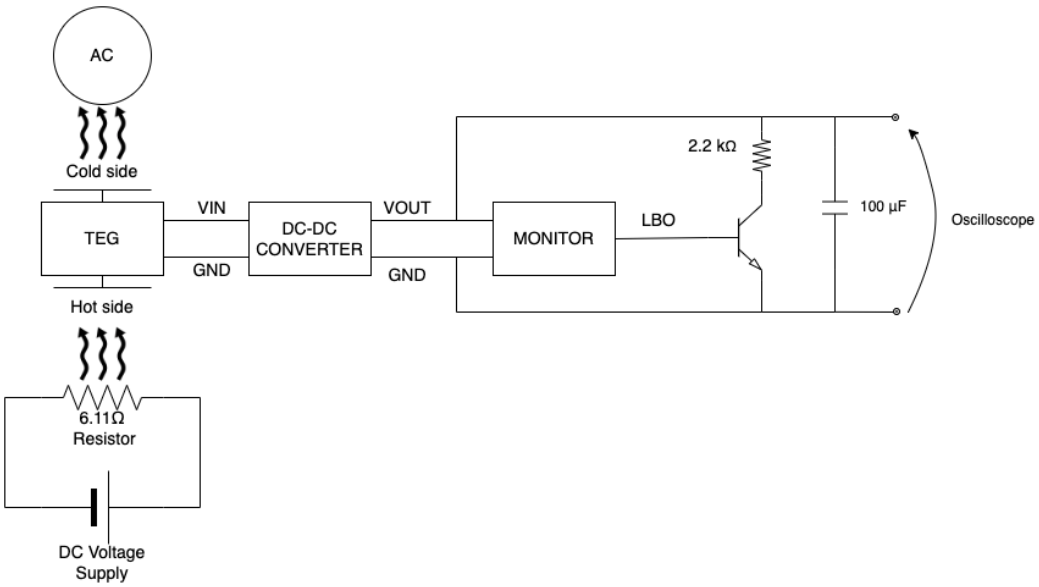

Figure 17: Maximum Transmit Burst Rate Measurement Set-Up

Maximum Transmit Burst Rate Results

Lowering the supplied DC voltage, we can reduce the temperature gradient. The Maximum Transmission Rate has been measured for 3 different temperature gradients.

Figure 18 shows that with a 0.7 K temperature gradient, the system can endure a maximum transmission rate of 10 seconds.

Figure 19 shows that with a 0.45 K temperature gradient, the system can endure a maximum transmission rate of 30 seconds.

Figure 20 shows that with a 0.3 K temperature gradient, the system can endure a maximum transmission rate of 60 seconds.

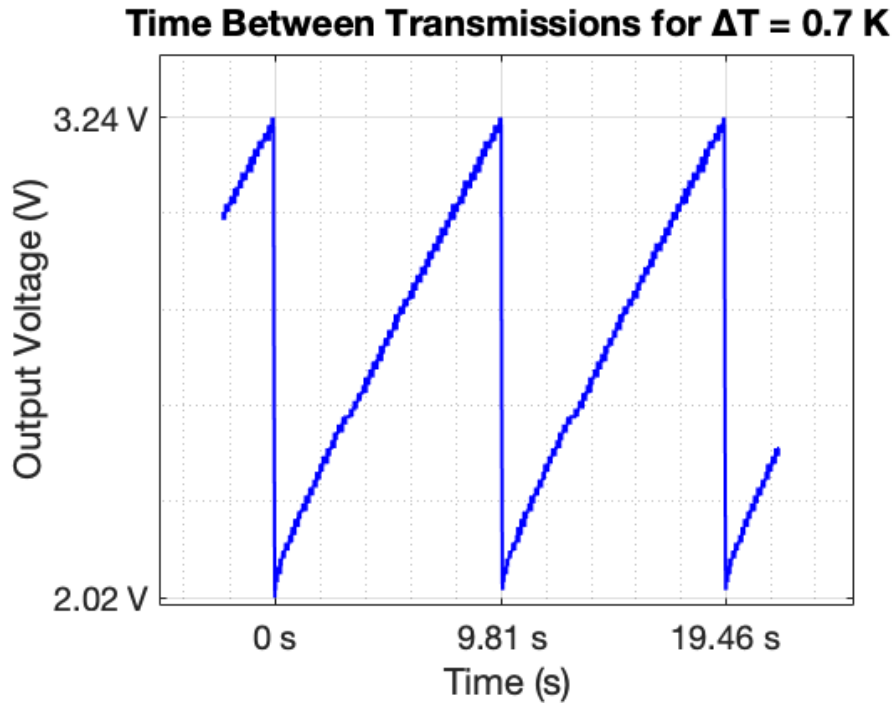

Figure 18: Approximately 10 second Transmit Burst Rate with a 0.7 K gradient

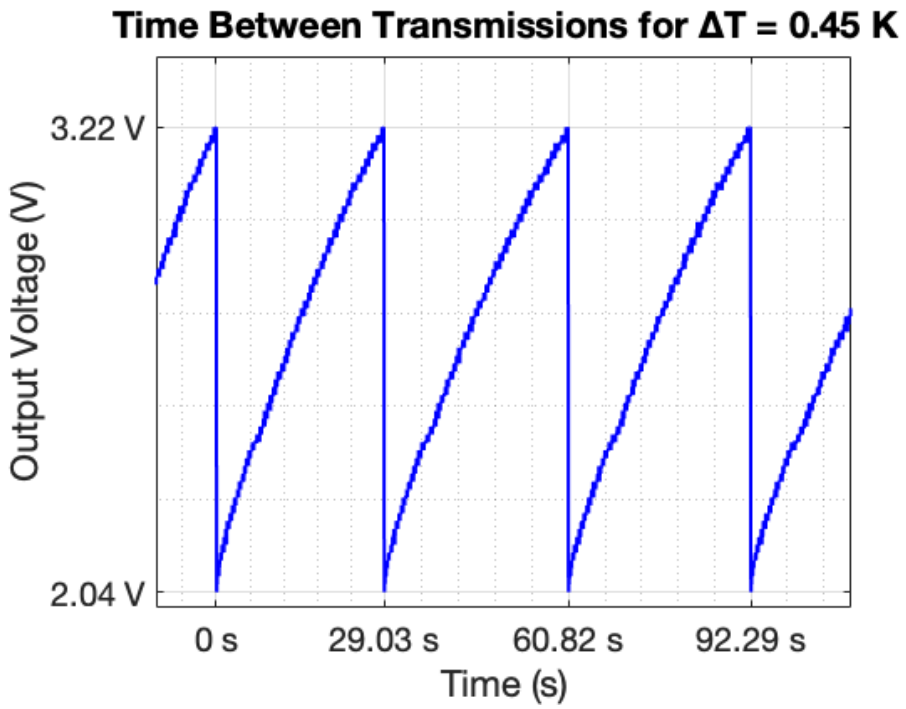

Figure 19: Approximately 30 second Transmit Burst Rate with a 0.45 K gradient

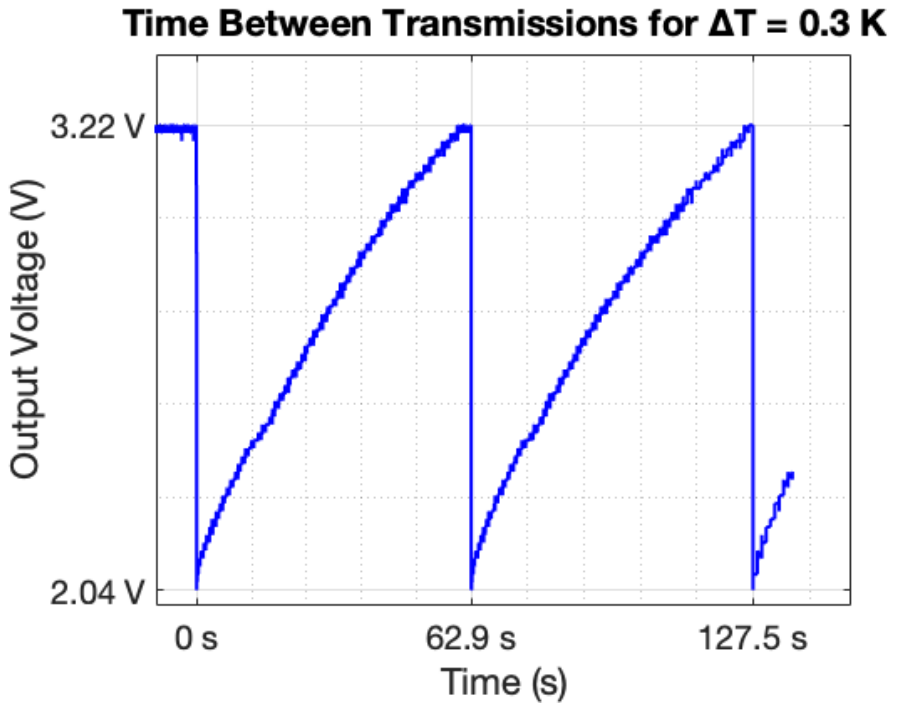

Figure 20: Approximately 60 second Transmit Burst Rate with a 0.3 K gradient

6.3. Summary and Redesign Criteria

In this chapter a design that includes the voltage converter module, the energy storage module, and the voltage monitor module has been presented and successfully validated for a TEG. An equivalent design has also been built for the solar cell, but again the desired results were not obtained. With the presented design the maximum transmit burst rate has been calculated.

The next chapter describes the third intermediate design. Following an incremental method it includes all the modules described in this chapter and the previous one (the voltage converter, the energy storage capacitor, and the voltage monitor modules) and adds a switch module to it. The third design has been only made for the TEG harvester, since the solar cell has been discarded as a power source due to its issues.

7. DESIGN 3: THE SWITCH

In this chapter, the two chosen switches are tested and characterized, to select the most adequate for the third design, which is already a complete provisional PMU. The first, is a NPN BJT available in the laboratory where this project has taken place. The second, is a SN74LVC1G66-Q1, which is single bilateral analog switch manufactured by Texas Instruments. In this chapter, the voltage drop across both switches in ON and OFF state has been measured and compared. Additionally, with the provisional PMU version, the complete long-range harvester-assisted wireless sensor node has been validated.

Figure 21 shows the block diagram of the complete system. Thick black borders indicate that the block is included in this third intermediate design, while grey thin borders indicate that the block is not included in the design. The diagram shows how the provisional PMU is completed in this design.

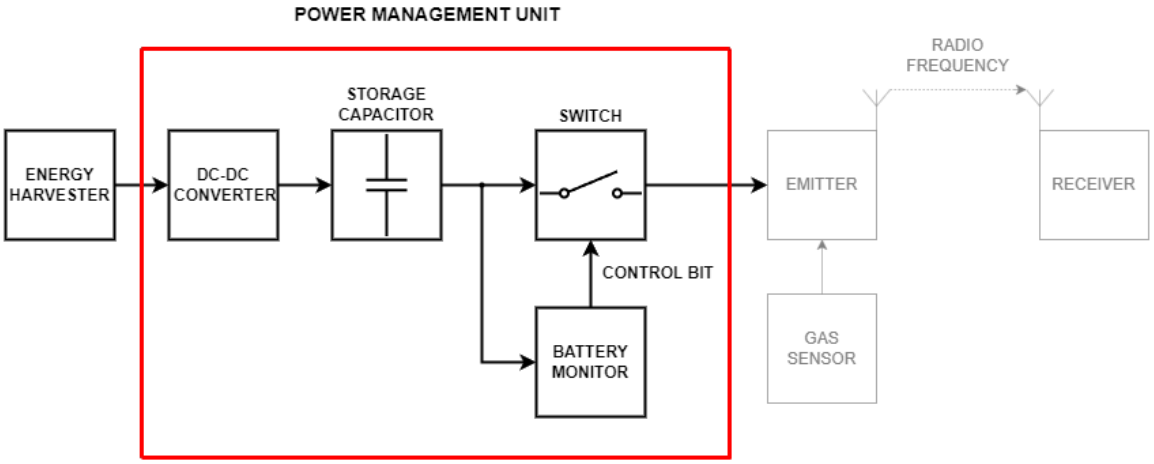

Figure 21: Design 3 Block Diagram: the PMU

7.1. Switch Characterization

Two set-ups, one for the characterization of each switch, are proposed. In both cases, if the switches were ideal, the voltage drop across the resistor shown in Figures 22 and 23 should be of 0 V when the switch is open, and 3.3 V when it is closed. The switch should be open while the control pulse is low, and closed when it is high.

7.1.1. BJT Characterization Set-Up

Figure 22 shows the set up used for the characterization of the BJT switch.

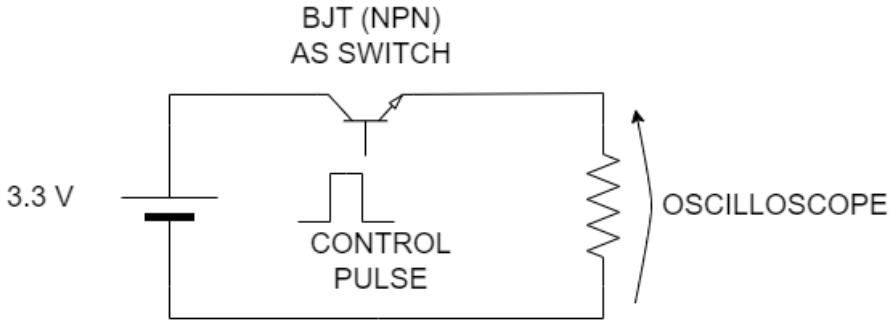

Figure 22: BJT Switch Characterization Set Up

7.1.2. SN74LVC1G66-Q1 Characterization Set-Up

Figure 23 shows the set up used for the characterization of the SN74LVC1G66-Q1 switch.

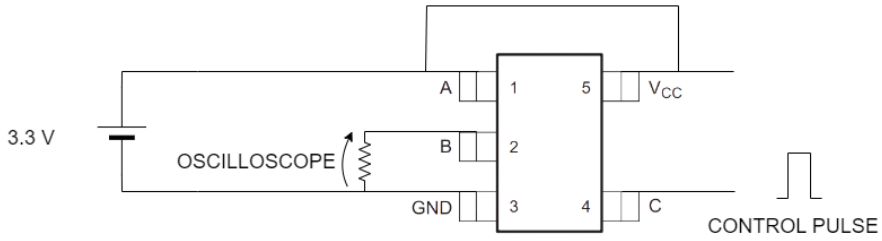

Figure 23: SN74LVC1G66-Q1 Switch Characterization Set Up

7.1.3. Characterization Results

It is possible to observe in Figure 24 that the switches do not respond the same way. Figure 24a shows the result of characterizing the BJT switch, while 24b shows the result of characterizing the SN74LVC1G66-Q1. Both are able to completely open when the control pin is LOW (ensuring that the current across the resistor is equal to zero). However, when the control pin is HIGH, the voltage drop across the BJT switch is of 0.66 V (3.3 - 2.64), while the voltage drop across the SN74LVC1G66-Q1 is negligible. In Figure 24b the voltage changes value several times before definitively dropping to 0 V. The connections to obtain this graph were done using a breadboard, and this anomaly is due to the cable that controls the switch losing and regaining contact while being pulled out. This could have been solved with a filter, but it was not considered necessary for the characterization of the switch.

It is possible to test now both switches, using the LBO output of the monitor as the control pulse, and the DC-DC step-up converters output voltage as the voltage source.

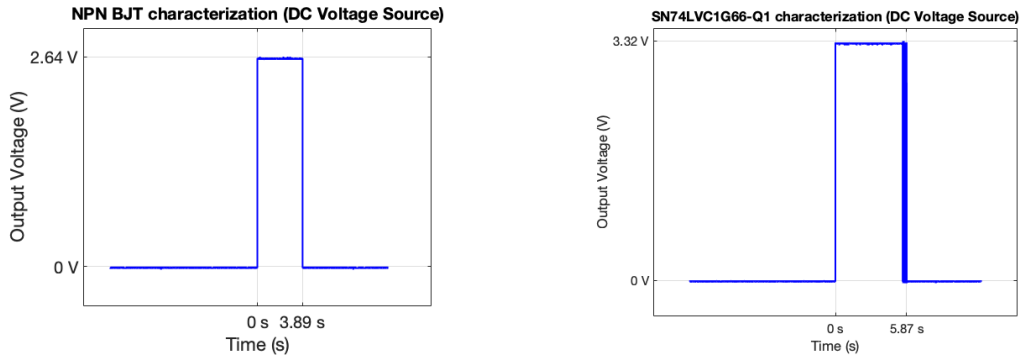

(a) BJT Switch (b) SN74LVC1G66-Q1

Figure 24: Switch Characterization

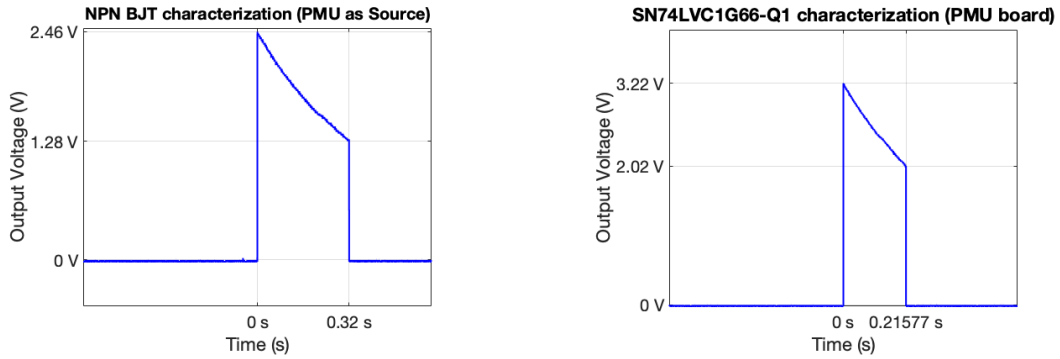

(a) BJT Switch (b) SN74LVC1G66-Q1

Figure 25: Switch Testing

Figure 25 shows the result of this test. Figure 25a shows the result using the BJT switch, while Figure 25b shows the result of using the SN74LVC1G66-Q1. Again, there is a noticeable voltage drop across the BJT switch, while it is negligible across the SN74LVC1G66-Q1.

We can also observe that the voltage is not constant during the ON state. This is due to the discharge of the capacitor. The LBO pin is HIGH from the moment the voltage provided by the capacitor reaches 3.22 V, until it gets lower than 2.02 V. The time it takes the capacitor to discharge depends on the load, which is a 2.2 kΩ resistor in this case, and of the temperature gradient across the TEG.

7.2. Design 3 Proposal

Having chosen the SN74LVC1G66-Q1, the Design 3 has been built connecting the switch to the second design with cables. Figure 26 shows the proposed design. To connect the second design with the switch it is necessary to short circuit pins 1 and 5 and connect them to the VOUT pin of the LTC3108. Pin 3 is connected to the GND of the board, and pin 4 is connected to the LBO pin of the MAX6433. With the selected switch, the Power Management Unit is completed, and its output is pin 2, referenced to the GND pin. Since only one component was added to the previous design, no PCB has been built in this case.

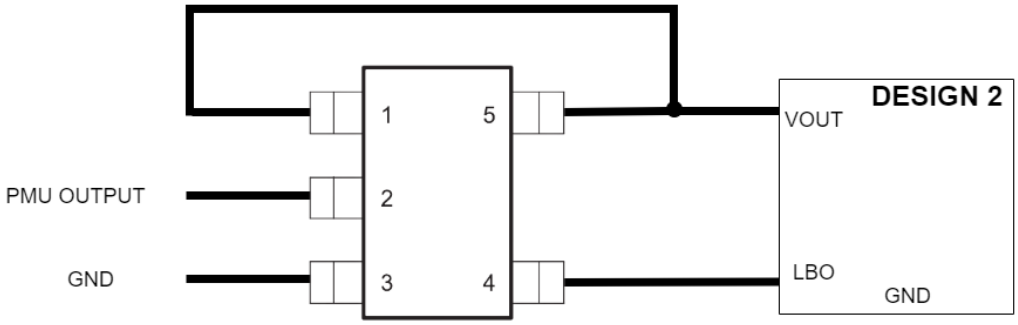

Figure 26: The SN74LVC1G66-Q1 Switch [21] Implementation

7.3. Design 3 Validation

A test connecting the PMU to the sensor node has been carried out to validate the third design.

7.3.1. Design 3 Validation Set-Up

The third design has been tested connecting the output of the PMU, this is, pin 2 in Figure 26, to the 3V3 pin of the LAUNCHXL-CC1310 Evaluation Board, and connecting their GND pins with cables. The LAUNCHXL-CC1310 has its DIO7 pin supplying power to the sensor module while the DIO23 pin receives the output of the sensor.

Figure 27 shows the pin distribution of the LAUNCHXL-CC1310 Evaluation Board.

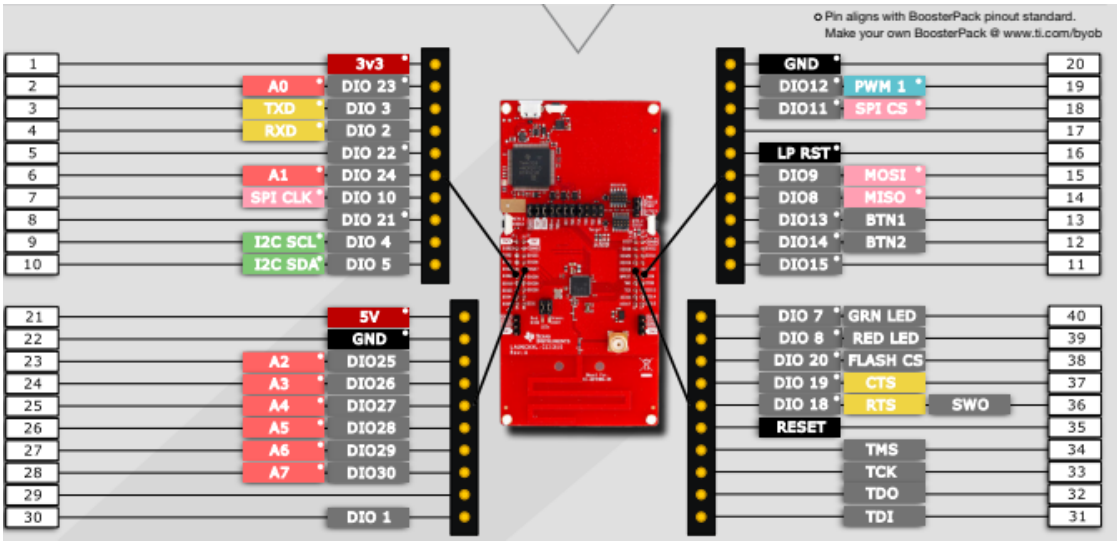

Figure 27: LAUNCHXL-CC1310 Evaluation Board [24]

7.3.2. Design 3 Validation Results

The results of testing the third design to the rest of the sensor node was that the system was capable of periodically sending the information read from the sensor with only a TEG as a power supply. The temperature gradient across the TEG was generated in the same way as in previous Set-Ups (see Figure 7) This way, the design of the PMU was successfully validated. No extra capacitor was required for the transmissions.

7.4. Summary and Redesign Criteria

In this chapter the SN74LVC1G66-Q1 has been selected for the switch module after comparing both available options. With the selected switch, a third intermediate design that completes a provisional PMU has been presented. This design has been tested and validated. Additionally, with the provisional PMU the complete long-range harvester-assisted wireless sensor node has been validated.

Chapter 8 presents a final design equivalent to the tested one in this chapter, but eliminating the cable connections and integrating all the modules that form the long-range harvester-assisted wireless sensor node in a single board. Moreover, the PMU has been simplified for its final design.

The simplifications that have been done are:

- Eliminating of the 0 Ω Resistors to directly connect VS1 to VAUX pin and VS2 to GND pin (all of the pins are referred to the LTC3108)
- Eliminating all the pin headers that were unused (JP1, JP2 and JP3 in Figure 16)
- Eliminating the space for the solar cells (BT1 and BT2 in Figure 16)
- Referencing the bottom layer to VOUT instead of VAUX (both pins are referred to the LTC3108)

8. PROPOSED SENSOR NODE DESIGN

In this chapter the solutions for the main objectives are proposed. First, the PCB for the complete long-range harvester-assisted wireless sensor node is presented. The final power management unit is integrated in that board, and it is also presented separately in this chapter.

The proposed power management unit is suit to supply a voltage between 3.22 V and 2.04 V to a long-range harvester-assisted wireless sensor node during transmissions of information, obtaining the energy to do so exclusively from a Thermoelectric Generator.

The design of the PMU has been done following an incremental iterative method. The previous chapters explained the different boards that have been designed and tested before obtaining the final design of the PMU that is presented in this chapter.

Figure 28 shows the block diagram of the complete sensor system. Blocks with thick black borders are included in the final autonomous sensor node design, while blocks with grey thin borders are not part of the final design.

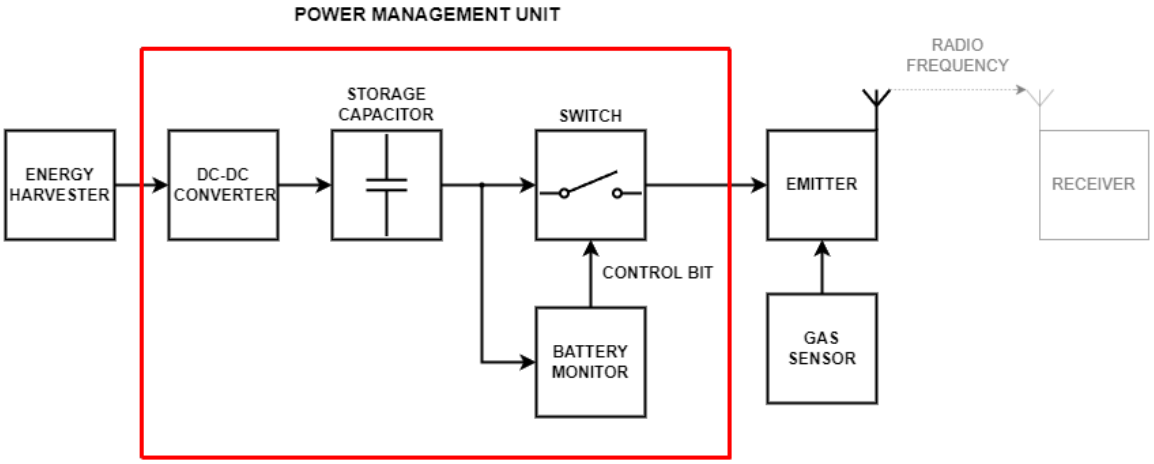

Figure 28: Long-Range Harvester-Assisted Wireless Sensor Node Block Diagram

8.1. The Complete Sensor Node

8.1.1. The PCB

Figure 29 shows the schematic of the design for the complete long-range harvester-assisted wireless sensor node. This design integrates the power management unit, the circuit required to read the information of the gas sensor, and all the required pins to connect it the LAUNCHXL-CC1310 Evaluation Board.

Figure 30 shows the final Printed Circuit Board where the emitter module, the sensor module and the PMU module of the long-range harvester-assisted wireless sensor node are integrated.

Figure 31 shows the final designed hardware where the all the modules for the complete autonomous sensor are included or can be connected.

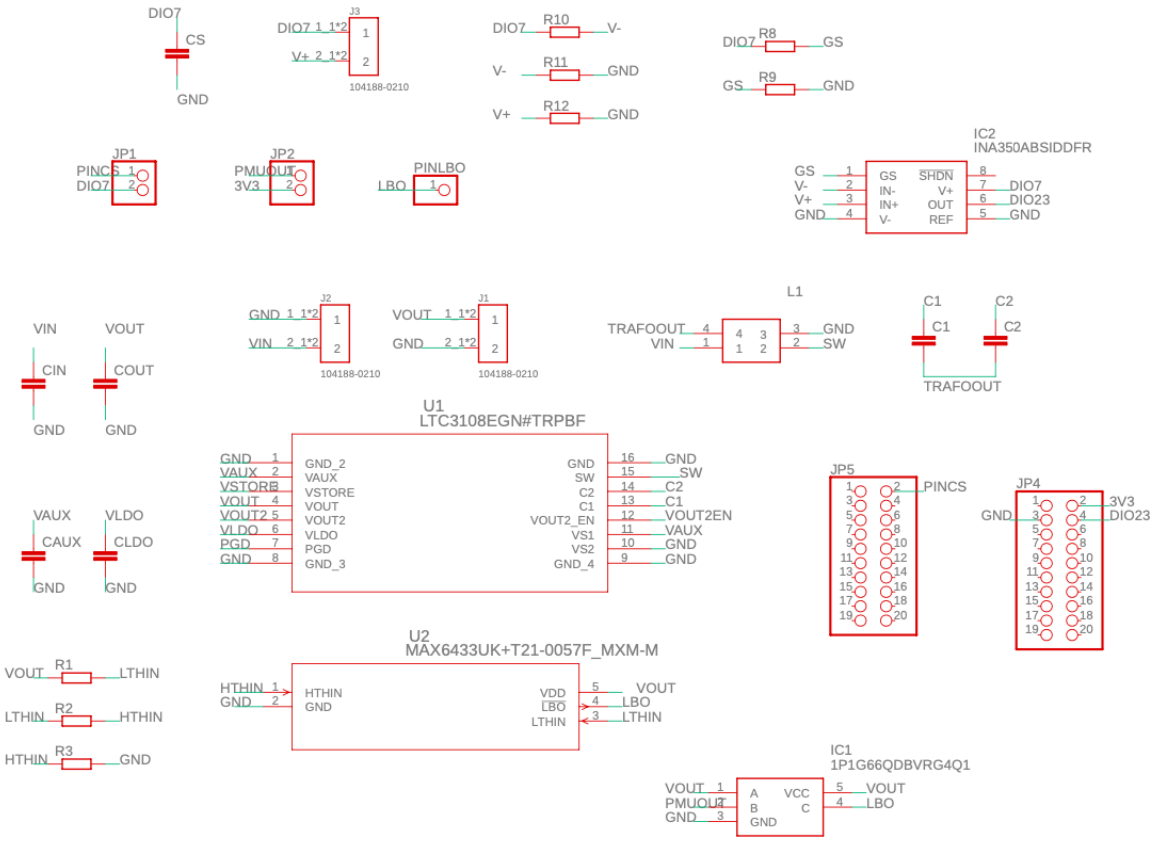

Figure 29: Schematics of the Long-Range Harvester-Assisted Wireless Sensor Node

This board has been designed in collaboration with Aiora Etxeburua, who was in charge of designing the sensor module, and Mario Ibarrola, who was in charge of the emitter module.

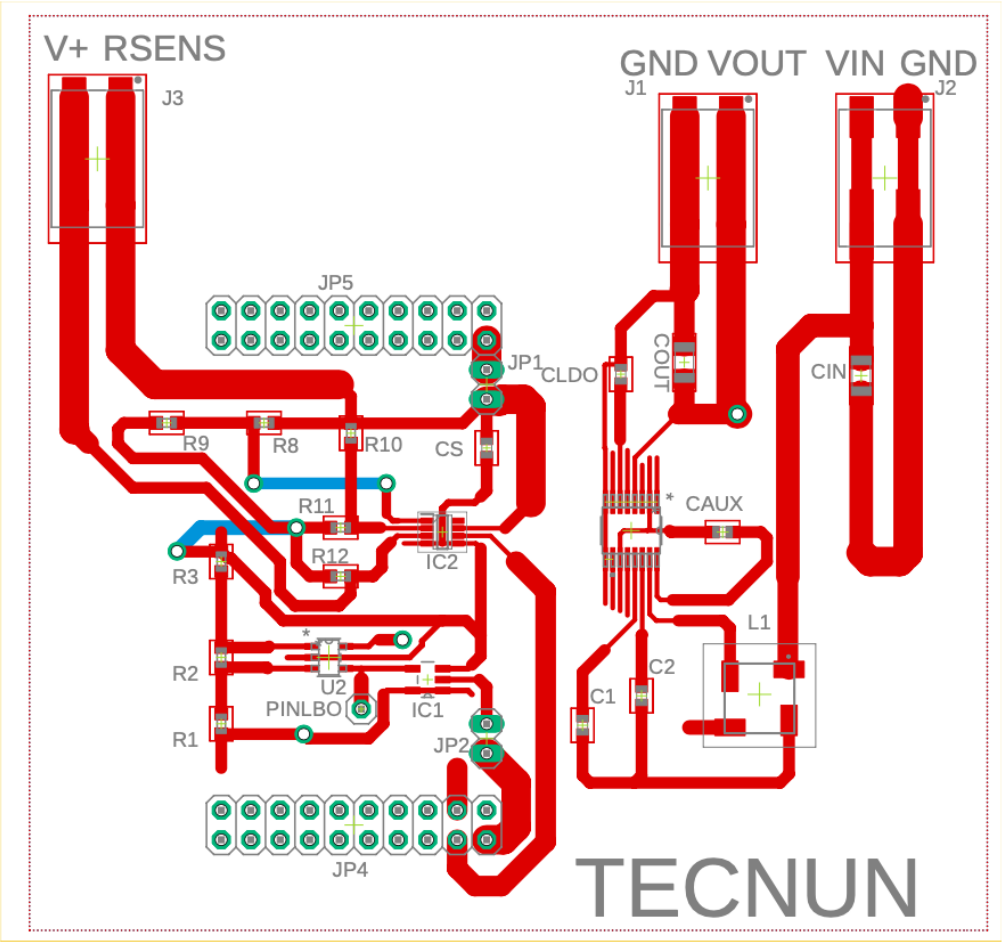

Figure 30: PCB for the Long-Range Harvester-Assisted Wireless Sensor Node

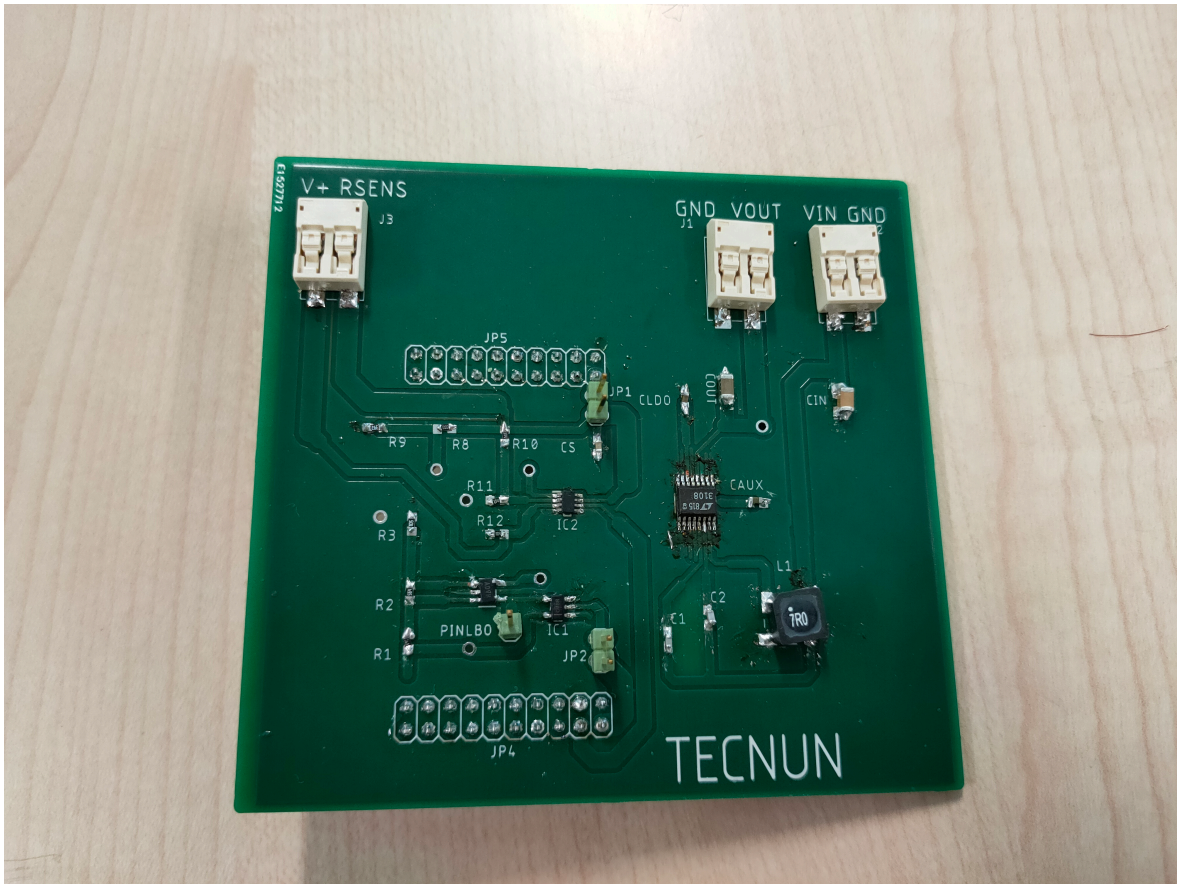

Figure 31: Designed Hardware

8.1.2. Components

Table 5 shows the Bill of Materials (BOM) needed to complete the final long-range harvester-assisted wireless sensor node. The left column specifies the module to which each of the components belongs. The second column shows the name that indicates the position of the component on both the schematic and the board [Figures 29 and 30]. The third column shows a description of the component. The fourth column shows the reference name of the component. Finally, the right column indicates the price of the component.

The selection of the components that form the sensor module has been done by Aiora Etxeburua, and it is not the purpose of this project to explain it.

The DC-DC Converter Module, the Voltage Monitor Module and the Switch Module are the ones that form the Power Management Unit, and therefore the focus of this work. The selection of the components that form them has been explained in the previous chapters. Chapter 5 explained the selection of the components corresponding to the DC-DC Voltage Converter; Chapter 6, the selection of the components for the Voltage Monitor; and Chapter 7, the selection of the switch.

Module	Name on board	Description	Reference name	Price
Converter Module	CIN	220 µF, 1206 size capacitor	GRM31CR60G227ME11L	0.99 €
	COUT	100 µF, 1206 size capacitor	12066D107MAT2A	0.75 €
	L1	1:100 turn ratio Transformer	74488540070	3.57 €
	C1	1 nF, 0603 size capacitor	0603YC102J4T2A	0.24 €
	C2	330 pF, 0603 size capacitor	0603YA331JAT2A	0.28 €
	CAUX	3.3 µF, 0603 size capacitor	06036D335KAT2A	0.24 €
	CLDO	2.2 µF, 0603 size capacitor	06036D225KAT2A	0.16 €
	U1	DC-DC Voltage Converter	LTC3108IGN#PBF	9.79 €
Monitor Module	R1	3.6 MΩ, 0603 size resistor	CRCW06033M60JNEA	0.19 €
	R2	560 kΩ, 0603 size resistor	CRCW0603560KJNEA	0.09 €
	R3	1 MΩ, 0603 size resistor	CRGCQ0603J1M0	0.12 €
	U2	Voltage Monitor	MAX6433UK+T	3.97 €
Switch Module	IC1	Switch	1P1G66QDBVRG4Q1	0.48 €
Sensor Module	CS	100 nF, 0603 size capacitor	0603YC104J4T4A	0.31 €
	R8	33 kΩ, 0603 size resistor	CRGCQ0603J33K	0.12 €
	R9	3.9 kΩ, 0603 size resistor	CRCW06033K90JNTA	0.13 €
	R10	180 kΩ, 0603 size resistor	CRCW0603180KJNEA	0.09 €
	R11	180 kΩ, 0603 size resistor	CRCW0603180KJNEA	0.09 €
	R12	180 kΩ, 0603 size resistor	CRCW0603180KJNEA	0.09 €
	IC2	Instrumentation amplifier	INA350ABSIDDFR	0.59 €
Pins and Connectors	J3	Lite-trap connector	104188-0210	1.18 €
	J2	Lite-trap connector	104188-0210	1.18 €
	J1	Lite-trap connector	104188-0210	1.18 €
	PINLBO	1X1 male pin header	M22-2511005	0.07 €
	JP1	1X2 male pin headers	M22-2511005	0.14 €
	JP2	1X2 male pin headers	M22-2511005	0.14 €
	JP4	2X10 male pin headers	90131-0770	3.50 €
	JP5	2X10 male pin headers	90131-0770	3.50 €
Total Cost of Materials on a Single Board:				33.2 €

Table 5: Final Design Bill of Materials

It is important to notice that the 104188-0210 component is no longer available on the market, instead, the 2060-452/998-404 has been used as a reference for the price, since both are similar products. This price was checked in Reference [25]. The rest of the prices on the table were checked in Reference [26].

J3 is a connector where the sensor, which is a variable resistor, should be connected. J2 is the connector where the TEG can be connected. J1 is connector used only for measuring the output voltage of the DC-DC step-up converter.

PINLBO is a pin that can be used to check if the output bit of the monitor is HIGH or LOW.

JP1 and JP2 are each a pair of pins that can be connected together with jumpers. This way JP1 isolates the sensor module, and JP2 isolates the output of the PMU from the LAUNCHXL-CC1310 Evaluation Board. This board can be connected though the JP4 and

JP5 pins.

8.2. The Power Management Unit

The previous section showed the final board where the sensor module, the emitter module and the power management modules were integrated. In this section, the Power Management Unit is presented separately, since this module is the main focus of the project.

Figure 32 shows the separate schematic of the Power Management Unit, and Figure 33 shows its corresponding board. It is important to notice that this board has not been built. Figures 32 and 33 are taken from Figures 29 and 30 to only show the elements that correspond to the PMU in the long-range harvester-assisted wireless sensor node board.

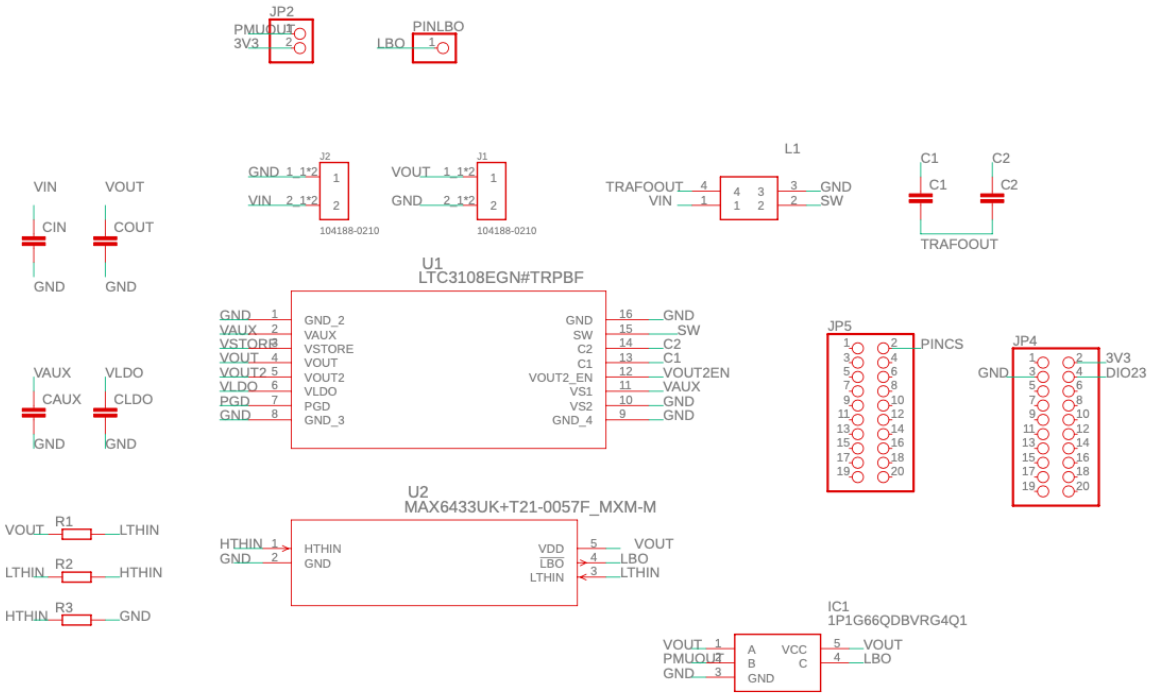

Figure 32: Schematics of the Power Management Unit

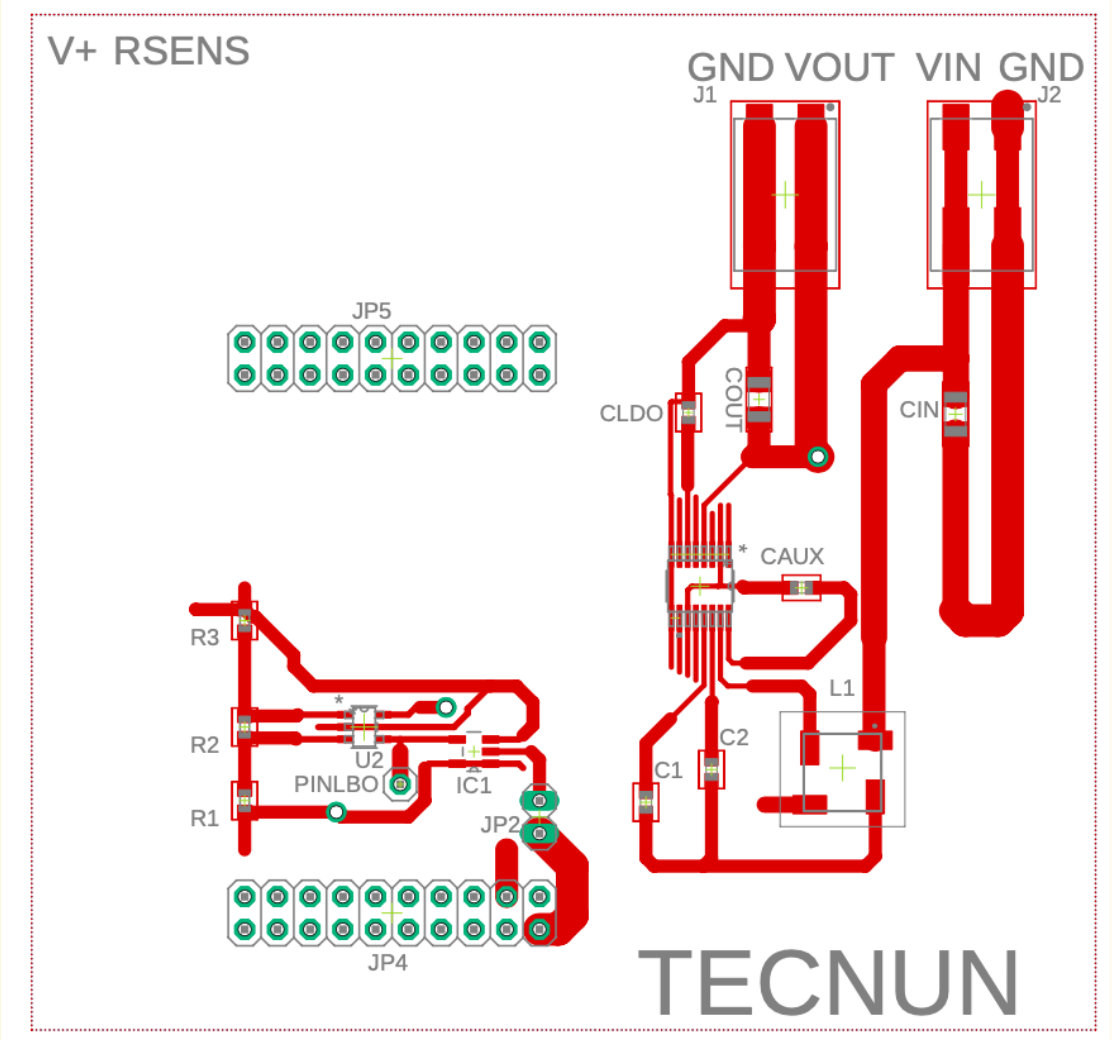

Figure 33: PCB for the Power Management Unit

9. CONCLUSION

The main objective of the project has been successfully accomplished: A Power Management Unit for the long-range harvester-assisted wireless sensor node has been successfully designed.

Additionally, the board for the complete long-range harvester-assisted sensor node has been designed and validated.

However, not all of the specifications or secondary objectives have been fully accomplished.

9.1. Design 1: The Voltage Converter and the Capacitor

The main objective of designing a module capable of adapting the output voltage of a harvester has been partially accomplished. A module designed for a TEG proved to be capable of boosting its output voltage up to 3.3 V, but the one designed for the Solar Cell did not work. The hypothesis proposed in this work, is that the solar cell was not able to provide enough power to make the DC-DC step-up converter start-up. A future study could analyze if this is true, and if perhaps a different solar cell model could have worked better. Another solution that could be analyzed is using more solar cells connected in series.

The main parameters were tested and characterized in the design for the TEG. However, analyzing the thermal noise it was observed that it was sufficiently high to potentially have altered the results of measuring the maximum output current with different temperature gradients and the output capacitor charging time. The latter was in fact incoherent with the theoretical expected result. A higher value resistor load should help the capacitor charge faster, because less power should be consumed by the load. However, this did not occur with the 5 MΩ and the 2 MΩ resistors. Instead, the capacitor charged faster with the lower value resistor. The hypothesis proposed in this work, is that thermal noise made the harvester provide more power when the measurement with the lower value resistor was carried out. A future study could analyze if this hypothesis is true. More reliable results could be obtained in an environment where the temperature of the hot and the cold side of the TEG could be controlled with more precision.

Since the solar cell did not work, the conclusion regarding which harvester was more adequate is that the TEG was better suit for the purpose of the project.

The final validation of the device proved that the 100 µF included on the voltage converter

module was enough to store the required energy for a transmission, so no extra capacitor in parallel is needed.

9.2. Design 2: The Battery Monitor

A second board adding the battery monitor was successfully designed. Moreover, the environmental conditions that ensured that at least one transmission per minute could occur were analyzed. Again, the results could have been more reliable if the temperature gradient on the TEG could be better controlled.

The main parameters were tested and characterized correctly. The total value of the resistors required for the external circuitry of the voltage monitor (the sum of the chosen R1, R2, and R3) was slightly higher than the recommended one in the MAX6433 Data Sheet [19]. The value with the chosen resistors was of 5.16 MΩ, while the recommended value was of 5 MΩ. With those resistors, theoretically the higher threshold (the output voltage of the converter at which the output bit of the monitor turned HIGH) should be 3.02 V, and the lower threshold (the output voltage of the converter at which the output bit of the monitor should turn LOW) should be of 2.03 V . However, the actual measurements showed that the output bit of the monitor turned HIGH when the output voltage of the converter was of 3.22 V, and LOW when it was 2.04 V. The first hypothesis proposed in this project to explain this difference is that the tolerance of the chosen resistors was high enough (5 %) to alter the threshold voltages. The second hypothesis is that the total sum of the resistors being 5.16 MΩ instead of 5Ω, as recommended on the Data Sheet, caused the difference between the theoritical and the experimental values. Either way, no changes were made because the real thresholds were considered adequate for our purpose. In fact, considering the available resistors and that an objective was to maximize the value of the total resistor (to reduce consumption), 3.02 V was the highest possible voltage value that was reachable. 3.22 V was therefore actually a better result than the expected one, since it was closer to 3.3 V while not being high enough to prevent the switch from closing when the capacitor reached its maximum voltage. Nevertheless, if a less fortuitous result was desired, resistors with closer values to the initially calculated ones, and with lower tolerances could be chosen.

9.3. Design 3: The Switch

A switch with a minimum voltage drop across it when closed, and a minimum current through it when opened was found and added to the final design. With this final module included, the final design of the PMU was proposed.

10. BUDGET

In this chapter, the budget corresponding to the development of the project is presented.

10.1. Cost of Labor

10.1.1. Cost of Labor to Build Final Device

Table 6 shows the detailed costs of the workers that are required to build the final device. The time it takes to build it is mainly related to the time it takes to solder all the components to the PCB.

Cost of Labor to Build Final Device

Task	Duration (hours)	Cost per Hour (€)	Total (€)
Junior Engineer	5 h	40.00 €	200.00 €
Total:			**200.00 €**

Table 6: Cost of Labor to Build Final Device

10.1.2. Total Cost of Labor

Table 7 shows the detailed costs of the workers that have participated in this project.

Cost of Labor for the Complete Project

Task	Duration (hours)	Cost per Hour (€)	Total (€)
Junior Engineer	300 h	40.00 €	12,000.00 €
Senior Engineer	50 h	100.00 €	5,000.00 €
Total:			**17,000.00 €**

Table 7: Total Cost of Labor

10.2. Budget Summary

10.2.1. Final Device Budget Summary

Table 8 shows the budget summary to build the final device. In this table, the price of the PCB has been determined by the estimation calculated with the help of Reference [27].

Final Device Budget Summary

Item	**Costs (€)**
Components	33.20 €
PCB	5.19 €
Labor	200.00 €
Indirect Costs (20%)	47.68 €
Total Cost of the Final Device:	**286.07 €**

Table 8: Total Cost of Final Device

10.2.2. Project Budget Summary

Table 9 shows the budget summary of the project.

Project Budget Summary

Item	**Costs (€)**
Fungible Materials	1,000.00 €
Labor	17,000.00 €
Indirect Costs (20%)	3,600.00 €
Total Cost of the Project:	**21,600.00 €**

Table 9: Project Budget Summary

REFERENCES

[1] Karen Rose, Scott Eldridge, and Lyman Chapin. "The internet of things: An overview". In: *The internet society (ISOC)* 80 (2015), pp. 1–50.

[2] Frederick J. Riggins and Samuel Fosso Wamba. "Research Directions on the Adoption, Usage, and Impact of the Internet of Things through the Use of Big Data Analytics". In: *2015 48th Hawaii International Conference on System Sciences*. 2015, pp. 1531–1540. DOI: 10.1109/HICSS.2015.186.

[3] Yusuf Perwej et al. "The internet of things (IoT) and its application domains". In: *International Journal of Computer Applications* 975.8887 (2019), p. 182.

[4] Sujesha Sudevalayam and Purushottam Kulkarni. "Energy Harvesting Sensor Nodes: Survey and Implications". In: *IEEE Communications Surveys Tutorials* 13.3 (2011), pp. 443–461. DOI: 10.1109/SURV.2011.060710.00094.

[5] Fayçal Ait Aoudia et al. "Leveraging Energy Harvesting and Wake-Up Receivers for Long-Term Wireless Sensor Networks". In: *Sensors* 18.5 (2018). ISSN: 1424-8220. DOI: 10.3390/s18051578. URL: https://www.mdpi.com/1424-8220/18/5/1578.

[6] M. T. Penella and M. Gasulla. "A Review of Commercial Energy Harvesters for Autonomous Sensors". In: *2007 IEEE Instrumentation Measurement Technology Conference IMTC 2007*. 2007, pp. 1–5. DOI: 10.1109/IMTC.2007.379234.

[7] Zhengguo Sheng et al. "A survey on the ietf protocol suite for the internet of things: standards, challenges, and opportunities". In: *IEEE Wireless Communications* 20.6 (2013), pp. 91–98. DOI: 10.1109/MWC.2013.6704479.

[8] Ko Ko Win et al. "Efficient solar energy harvester for wireless sensor nodes". In: *2010 IEEE International Conference on Communication Systems*. 2010, pp. 289–294. DOI: 10.1109/ICCS.2010.5686355.

[9] Loreto Mateu et al. "Energy harvesting for wireless communication systems using thermogenerators". In: *Proc. of the XXI Conference on Design of Circuits and Integrated Systems (DCIS), Barcelona, Spain*. 2006, pp. 22–24.

[10] Christopher M Vigorito, Deepak Ganesan, and Andrew G Barto. "Adaptive control of duty cycling in energy-harvesting wireless sensor networks". In: *2007 4th Annual IEEE communications society conference on sensor, mesh and ad hoc communications and networks*. IEEE. 2007, pp. 21–30.

[11] R.J.M. Vullers et al. "Micropower energy harvesting". In: *Solid-State Electronics* 53.7 (2009). Papers Selected from the 38th European Solid-State Device Research Conference – ESSDERC'08, pp. 684–693. ISSN: 0038-1101. DOI: https://doi.org/10.1016/j.sse.2008.12.011. URL: https://www.sciencedirect.com/science/article/pii/S0038110109000720.

[12] Amin Nozariasbmarz et al. "Review of wearable thermoelectric energy harvesting: From body temperature to electronic systems". In: *Applied Energy* 258 (2020), p. 114069.

[13] Mojtaba Forouzesh et al. "Step-Up DC–DC Converters: A Comprehensive Review of Voltage-Boosting Techniques, Topologies, and Applications". In: *IEEE Transactions on Power Electronics* 32.12 (2017), pp. 9143–9178. DOI: 10.1109/TPEL.2017.2652318.

[14] J. Biernacki and D. Czarkowski. "Radio frequency dc-dc flyback converter". In: *Proceedings of the 43rd IEEE Midwest Symposium on Circuits and Systems (Cat.No.CH37144)*. Vol. 1. 2000, 94–97 vol.1. DOI: 10.1109/MWSCAS.2000.951594.

[15] Fang Lin Luo and Hong Ye. *Advanced multi-quadrant operation DC/DC converters*. CRC Press, 2018.

[16] Eric J. Carlson, Kai Strunz, and Brian P. Otis. "A 20 mV Input Boost Converter With Efficient Digital Control for Thermoelectric Energy Harvesting". In: *IEEE Journal of Solid-State Circuits* 45.4 (2010), pp. 741–750. DOI: 10.1109/JSSC.2010.2042251.

[17] Anna Richelli et al. "A 0.2−1.2 V DC/DC Boost Converter for Power Harvesting Applications". In: *IEEE Transactions on Power Electronics* 24.6 (2009), pp. 1541–1546. DOI: 10.1109/TPEL.2009.2013224.

[18] Anna Richelli, Simone Comensoli, and Zsolt M. Kovacs-Vajna. "A DC/DC Boosting Technique and Power Management for Ultralow-Voltage Energy Harvesting Applications". In: *IEEE Transactions on Industrial Electronics* 59.6 (2012), pp. 2701–2708. DOI: 10.1109/TIE.2011.2167890.

[19] *MAX6427–MAX6438: Low-Power, Single/Dual-Level Battery Monitors with Hysteresis*. Maxim Integrated Products.

[20] Immanuel N Jiya and Rupert Gouws. "Overview of power electronic switches: A summary of the past, state-of-the-art and illumination of the future". In: *Micromachines* 11.12 (2020), p. 1116.

[21] *SN74LVC1G66-Q1 Single Bilateral Analog Switch*. Texas Instruments.

[22] Hector Solar et al. "A 22-m Operation Range Semi-Passive UHF RFID Sensor Tag With Flexible Thermoelectric Energy Harvester". In: *IEEE Sensors Journal* 22.20 (2022), pp. 19797–19808.

[23] *LTC3108: Ultralow Voltage Step-Up Converter and Power Manager Data Sheet*. Linear Technology.

[24] *CC1310 LaunchPad Getting Started Guide (Rev. B)*. Texas Instruments.

[25] *DigiKey*. https://www.digikey.es/. Accessed: July 15, 2023.

[26] *Mouser Electronics*. https://www.mouser.es/. Accessed: July 15, 2023.

[27] *PCBWay*. https://www.pcbway.com/QuickOrderOnline.aspx. Accessed: July 15, 2023.

A. VOUT CHARGING TIME GRAPHS

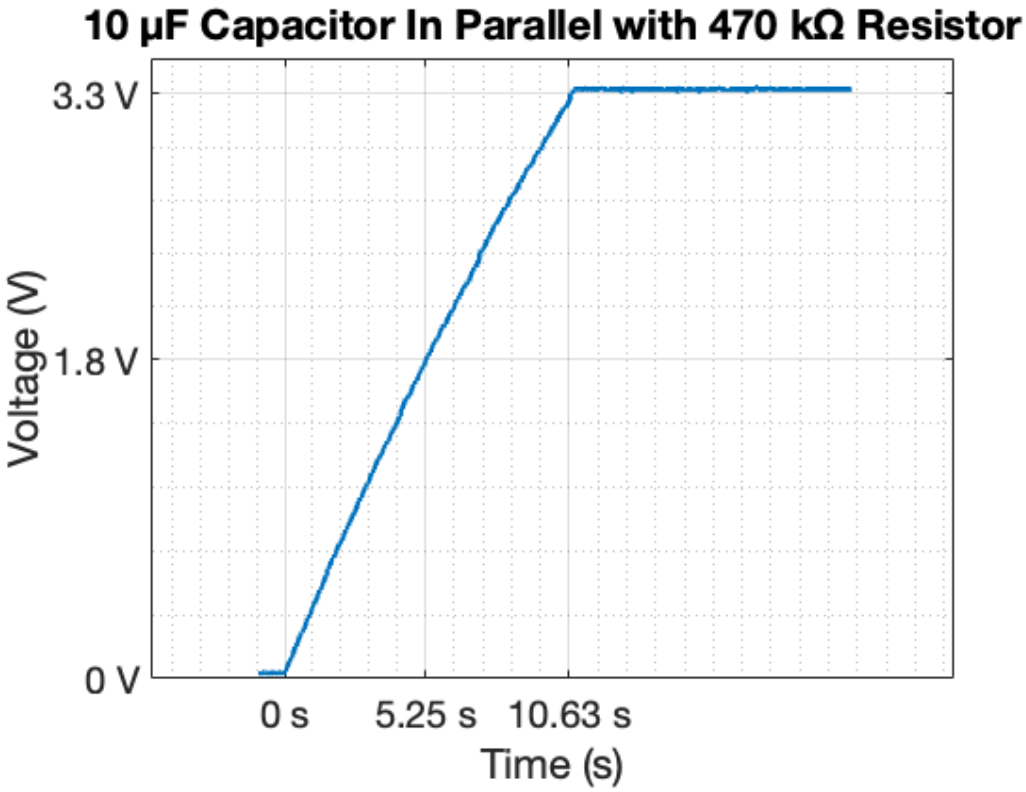

Figure 34: VOUT Charging Time with 10 µF Capacitor and 470 kΩ Resistor

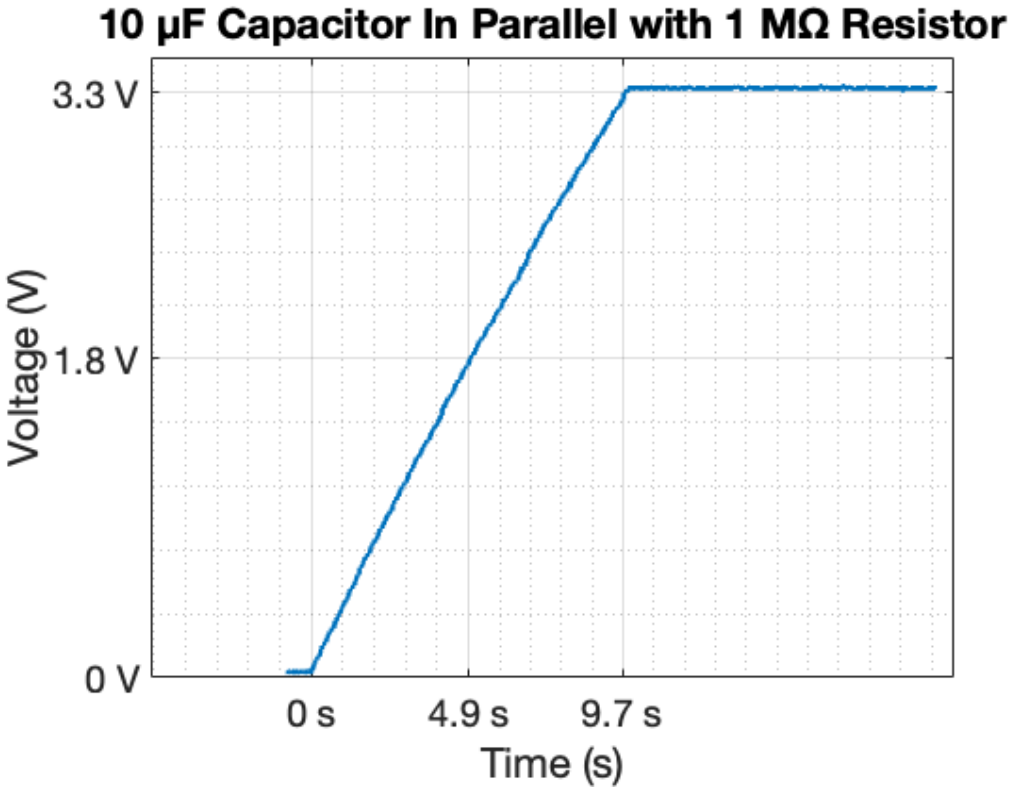

Figure 35: VOUT Charging Time with 10 µF Capacitor and 1 MΩ Resistor

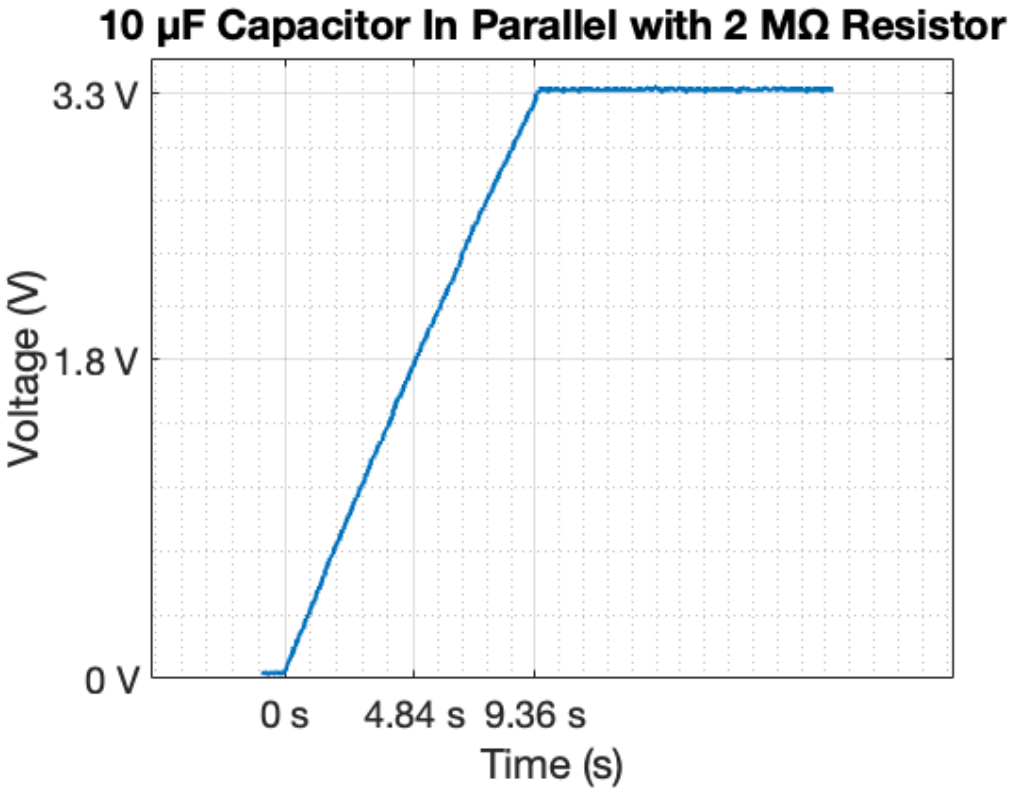

Figure 36: VOUT Charging Time with 10 µF Capacitor and 2 MΩ Resistor

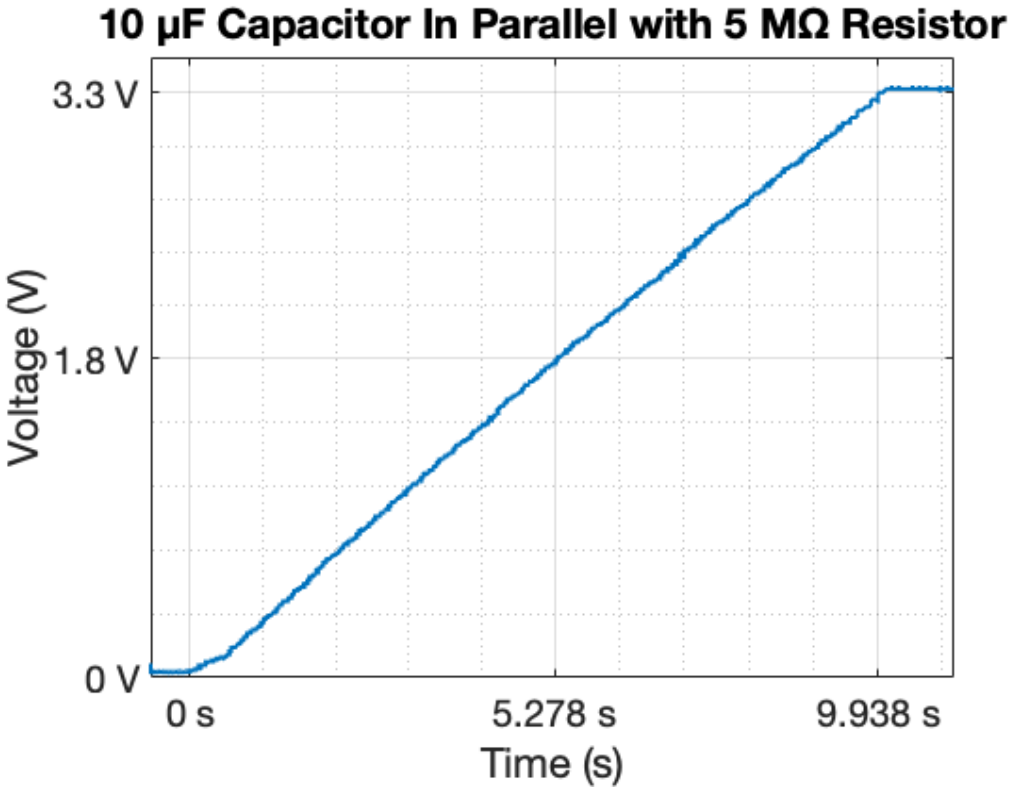

Figure 37: VOUT Charging Time with 10 µF Capacitor and 5 MΩ Resistor

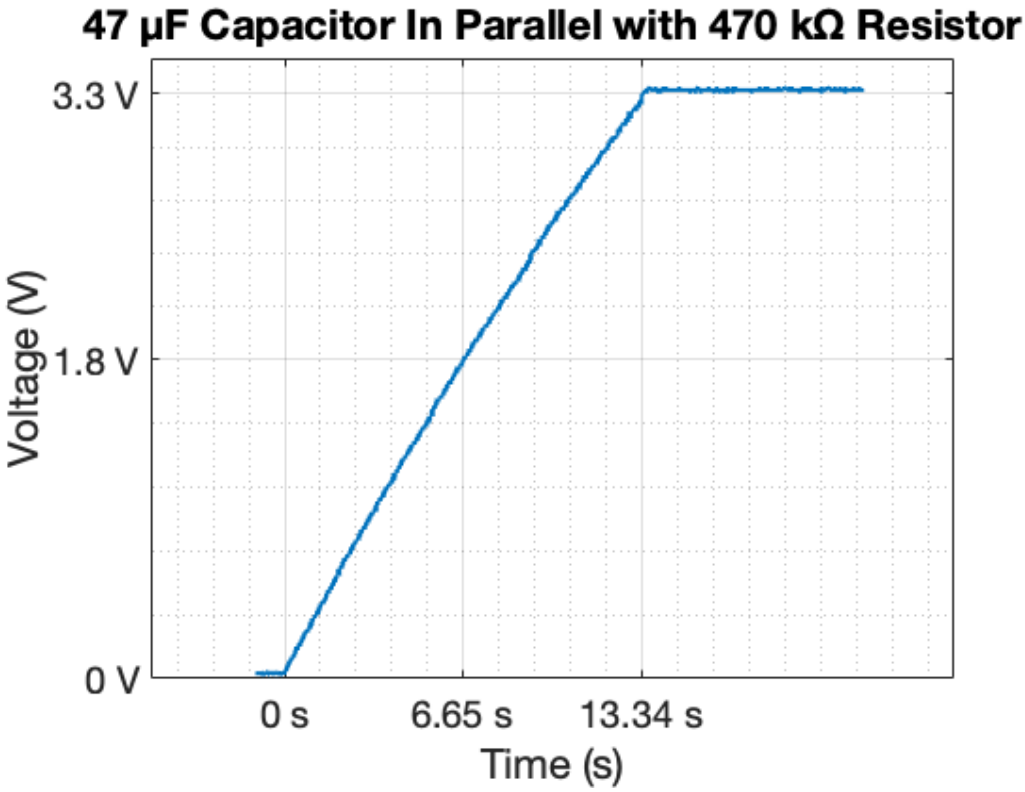

Figure 38: VOUT Charging Time with 47 µF Capacitor and 470 kΩ Resistor

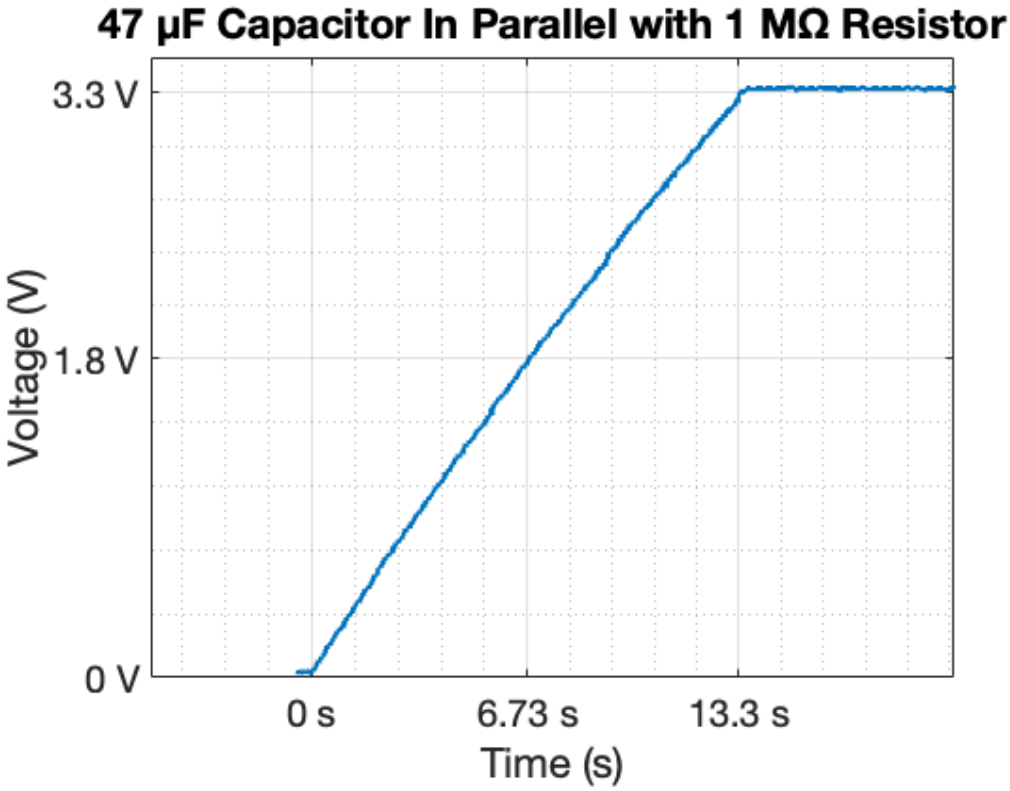

Figure 39: VOUT Charging Time with 47 µF Capacitor and 1 MΩ Resistor

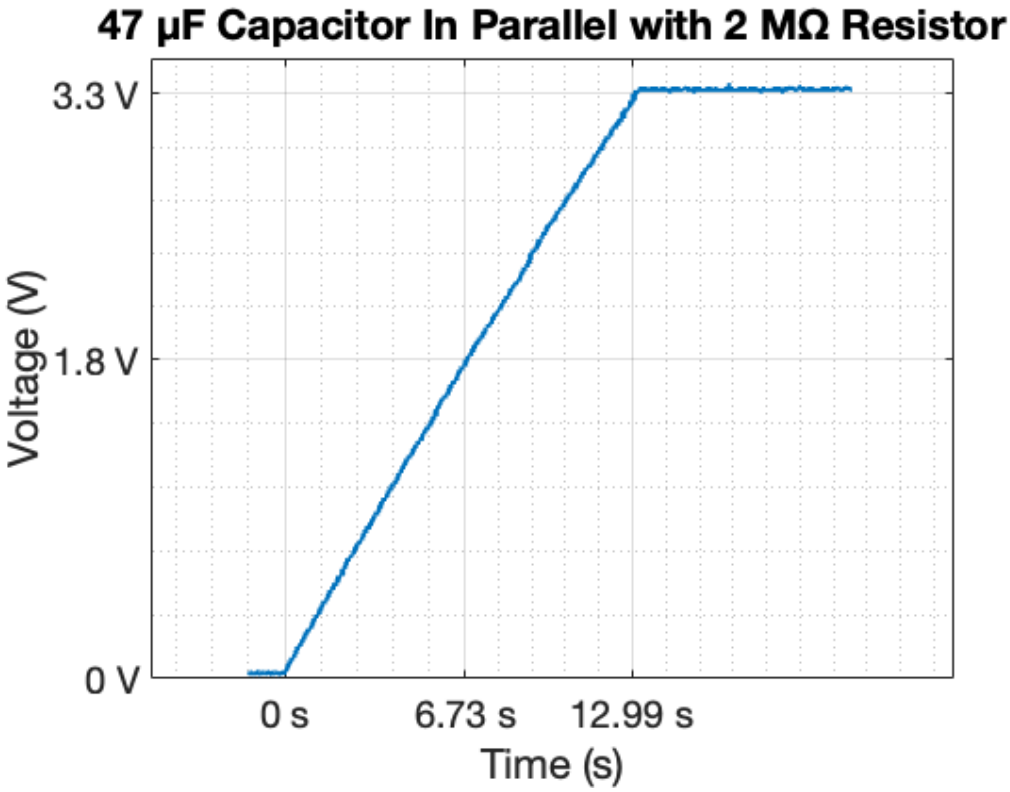

Figure 40: VOUT Charging Time with 47 µF Capacitor and 2 MΩ Resistor

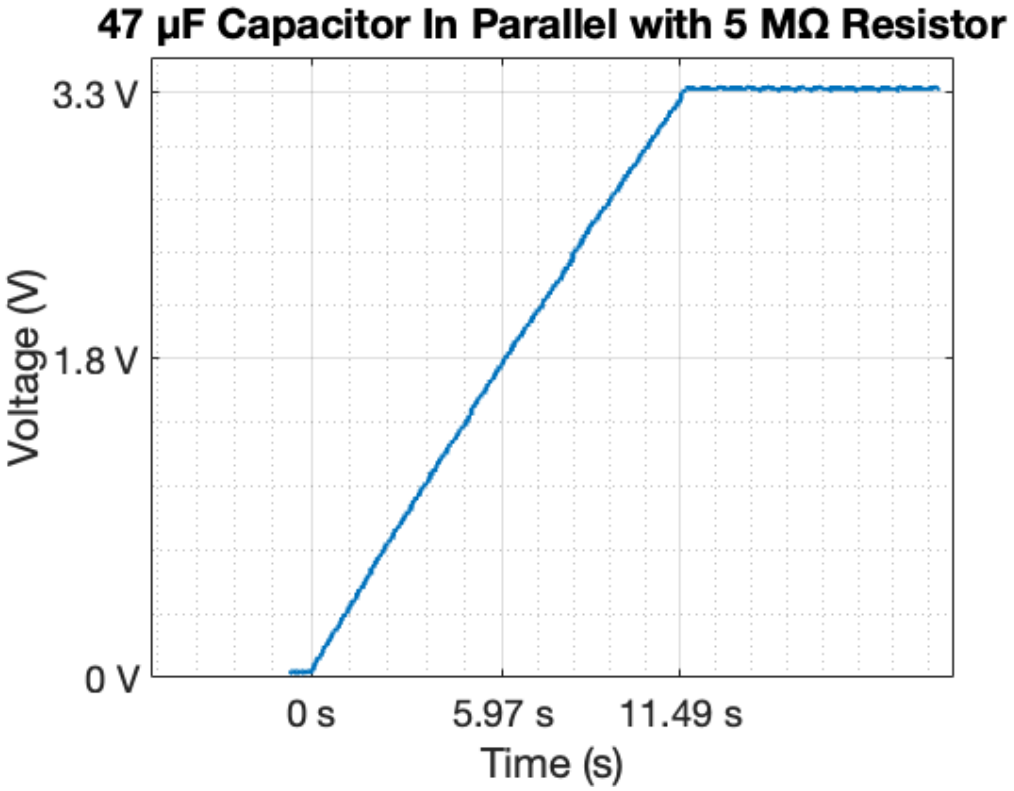

Figure 41: VOUT Charging Time with 47 µF Capacitor and 5 MΩ Resistor

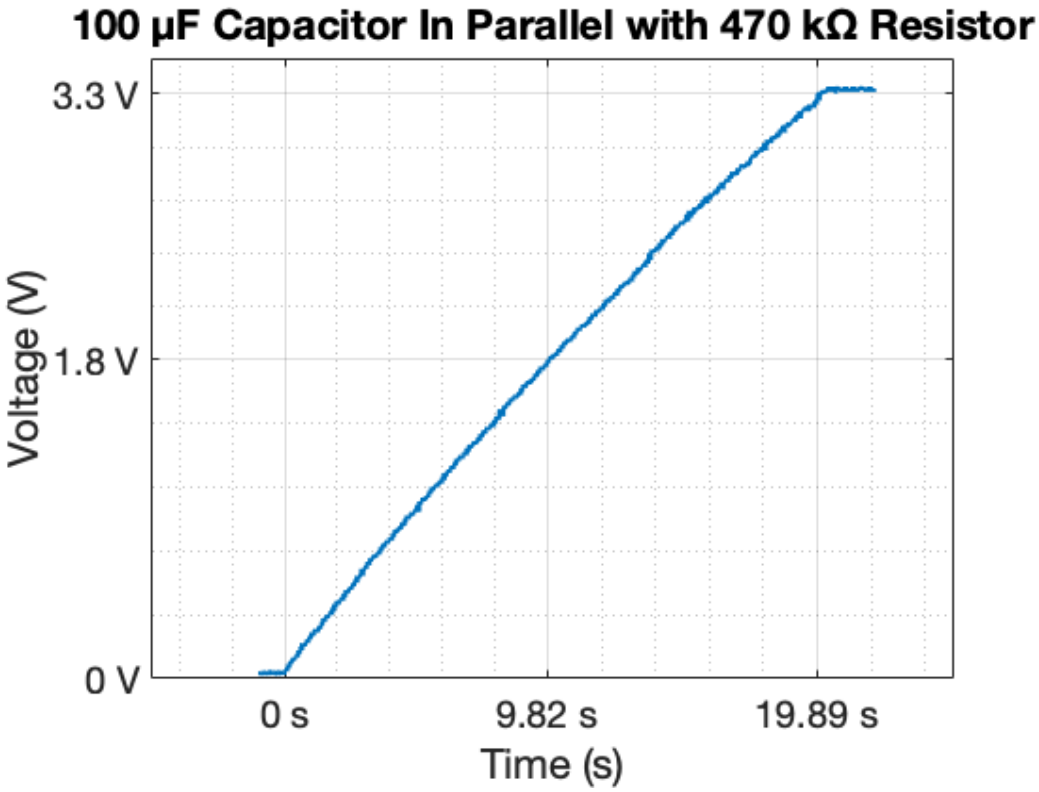

Figure 42: VOUT Charging Time with 100 µF Capacitor and 470 kΩ Resistor

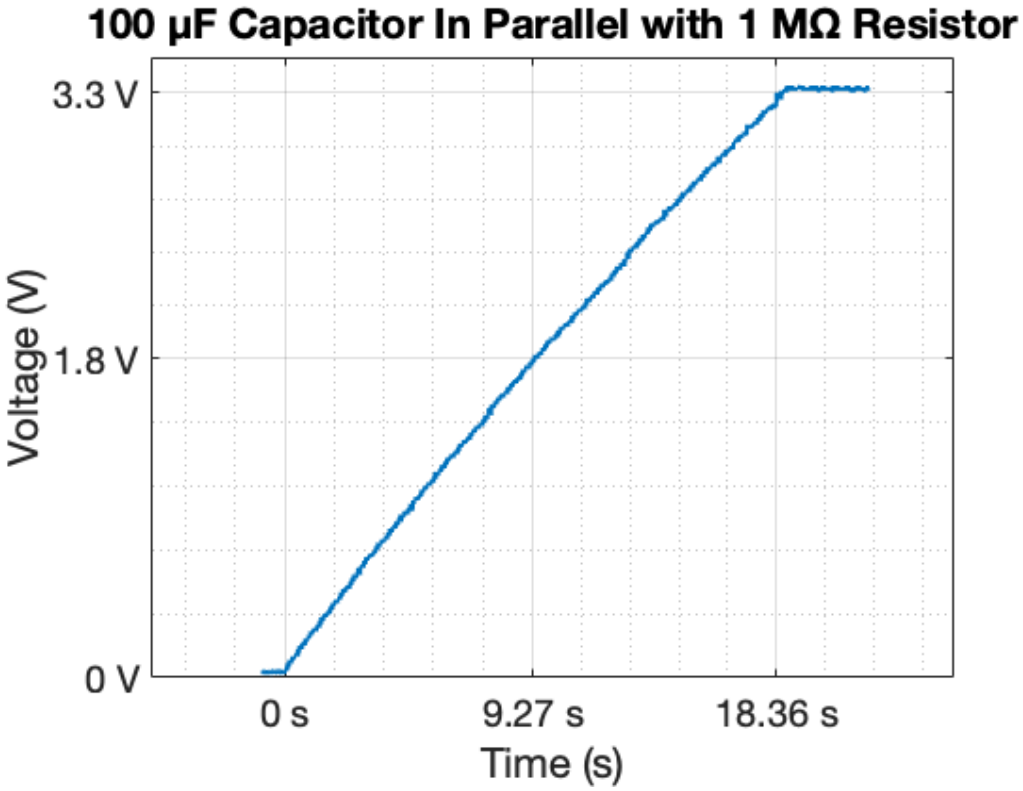

Figure 43: VOUT Charging Time with 100 µF Capacitor and 1 MΩ Resistor

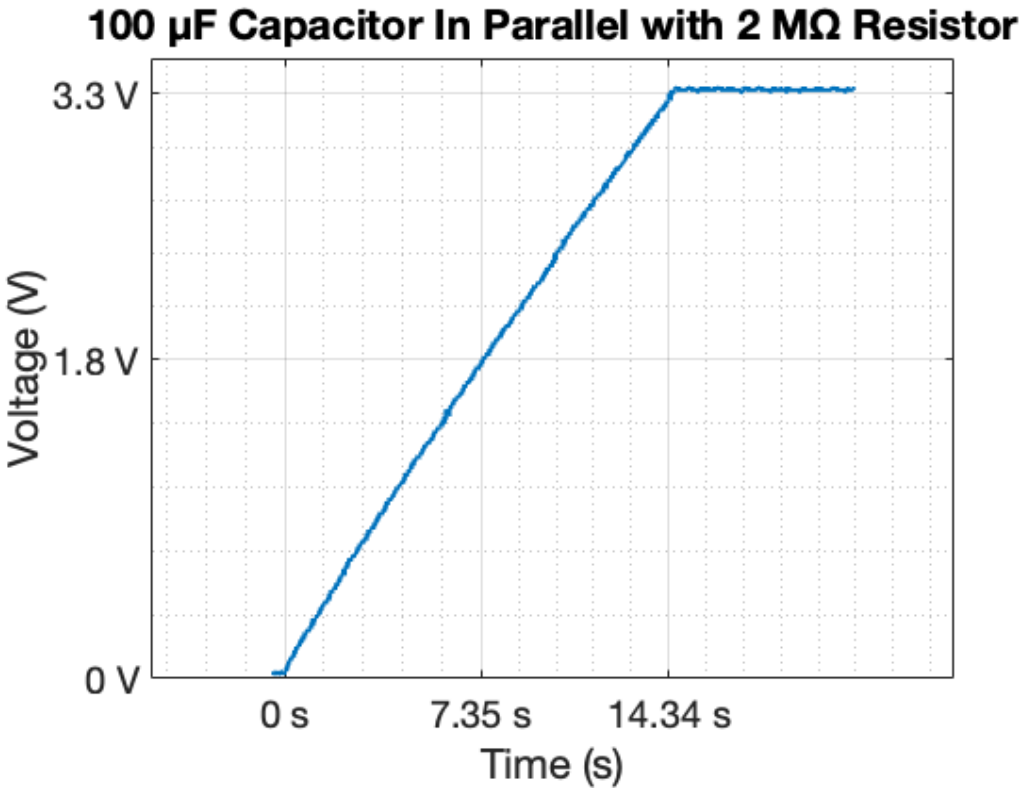

Figure 44: VOUT Charging Time with 100 µF Capacitor and 2 MΩ Resistor

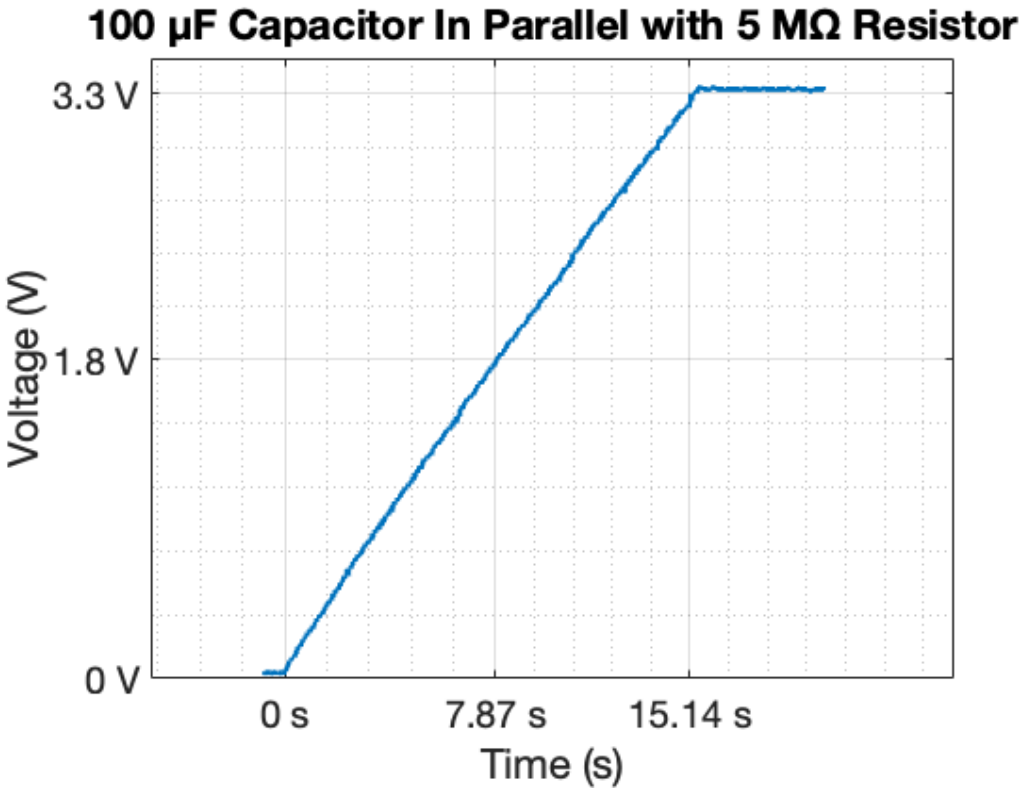

Figure 45: VOUT Charging Time with 100 µF Capacitor and 5 MΩ Resistor